The impact of the heteroatom in a five-membered ring on the photophysical properties of difluoroborates

Anna Grabarz, Beata Jędrzejewska, Agnieszka Skotnicka, N. Arul Murugan, Filip Patalas, Wojciech Bartkowiak, Denis Jacquemin, Borys Ośmialowski

The Impact of the Heteroatom in a Five-Membered Ring on the Photophysical Properties of Difluoroborates

Anna Grabarz[a], Beata Jędrzejewska[b], Agnieszka Skotnicka[b], N. Arul Murugan[c], Filip Patalas[d], Wojciech Bartkowiak[a], Denis Jacquemin[e,*], Borys Ośmiałowski[d,*]

[a] *Department of Physical and Quantum Chemistry, Faculty of Chemistry, Wrocław University of Technology, Wyb. Wyspiańskiego 27, PL–50370 Wrocław, Poland*
[b] *Faculty of Chemical Technology and Engineering, UTP University of Science and Technology, Seminaryjna 3, PL-85326 Bydgoszcz, Poland*
[c] *Division of Theoretical Chemistry and Biology, School of Biotechnology, Royal Institute of Technology, SE–10691 Stockholm, Sweden*
[d] *Faculty of Chemistry, Nicolaus Copernicus University, Gagarina 7, PL-87100 Toruń, Poland*
[e] *Laboratoire CEISAM, UMR CNRS 6230, Université de Nantes, 2 Rue de la Houssinière, BP92208, 44322 Cedex 3 Nantes, France*

Abstract

A series of novel BF_2 complexes, bearing a five-membered heterocyclic ring (with X=NMe, O, and S), were synthesized and characterized with a focus on the influence of atom exchange on the photophysical properties of both unsubstituted and dimethylamino derivatives. The experimental results show that the optical spectra substantially differ in both sets of dyes. In particular, the dimethylamino series are more strongly affected by heteroatom substitution, i.e., the insertion of X=O or X=S in lieu of X=NMe causes substantial bathochromic shifts of the absorption and emission bands, as well as marked changes in their topologies. In contrast, the optical spectra of the unsubstituted compounds undergo only relatively small redshifts, and no variation of band shapes is observed. Moreover, the measured absorption spectra of the unsubstituted compounds bearing X=NMe and X=O are almost identical. Interestingly, the fluorescence yields of the dimethylamino derivatives are much larger (up to one order of magnitude) than those of the corresponding unsubstituted compounds. The experimental analyses are supported by state-of-the-art quantum chemistry calculations, which satisfactorily reproduced the experimental trends and provided further insights into the observed optical signatures.

Keywords: TD-DFT, difluoroborates, functionalization, charge transfer

*Corresponding author
Email addresses: Denis.Jacquemin@univ-nantes.fr (Denis Jacquemin), borys.osmialowski@umk.pl (Borys Ośmiałowski)

1. Introduction

Structure-optical property relationships are now established for many classes of dyes, and one can often safely predict the evolution of absorption spectra with chemical substitution. This is more difficult to achieve for emission, which is a key challenge in view of its use in many biomedical imaging applications. Indeed, there is a need to design new fluorescent probes, effectively exhibiting sensitivity to environmental changes, physiological conditions and/or to specific interactions ongoing in biomacromolecules. To achieve these goals, countless syntheses have been carried out to functionalize fluorophores and tune their emissive properties, which can be achieved through standard variation of the substituent(s) [1–6], benzannulation [7–12], elongation of the π-conjugated spacer separating the donor and acceptor moieties in push-pull systems [13–17], or introduction of additional chromophores into their structure [18–20]. However, the addition of several substituents may lead to undesired effects such as the decrease of the fluorescence quantum yield (Φ_{fl}) inherent to flexible side group that enhance the efficiency of non-radiative pathways. This explains why the most potent fluorescent molecules remain "simple and rigid" derivatives, e.g., xanthenes [21–25], cyanines [26–30], BODIPYs [26; 31–35], and coumarins [36–40]. Among these classes, BODIPY derivatives occupy a privileged position [41], because they can be easily functionalized and are very photostable, explaining the undisputed popularity in this family [42–46]. However, one of the main disadvantages of regular BODIPY fluorophores is the impossibility to directly doubly-benzannulate their five-membered rings. Indeed, while single benzannulation has been achieved [47–49] and has shown to be an efficient strategy for red-shifting their absorption and fluorescence maxima, double benzannulation has only been achieved at other positions [50–53]. It is also well recognized that atom exchange, leading to isoelectronic compounds, may significantly impact the photophysical signatures of dyes. In fluoroborate dyes, substituent, benzannulation, and π-extension have been extensively applied to tune the photophysical properties, but atom exchange has been relatively less studied, though fluorescent techniques are also well suited to assess the impact of the

changes induced by atom-by-atom substitutions. In the classes of dyes encompassing atom-substituted BODIPYs, one should, of course mention: i) aza-BODIPY dyes – with a nitrogen atom at the *meso* position – that shows red-shifted optical bands compared to standard BODIPYs [54–58]; ii) other difluoroborates showing one or both nitrogen atoms in their N-BF_2-N core replaced by oxygen atoms, e.g., boranils [59–62], hydroxyphenyl-benzoxazole (HBO) complexes [63–65], difluoroboron β-diketonate complexes [66–68], and others [42; 69–71] (see Figure 1).

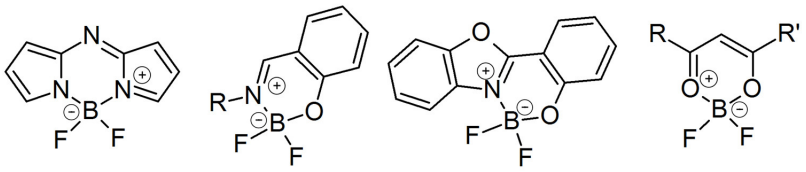

Figure 1: The common derivatives of BODIPY dyes, from left to right: aza-BODIPY, boranils, HBO complexes and difluoroboron β-diketonate complexes.

Notably, in contrast to standard BODIPY compounds, some of these derivatives, e.g., HBO complexes and boranils, are characterized by improved Stokes shifts (Δ_{ss}), usually larger than 50 nm [72–74], whereas the Δ_{ss} typically do not exceed 20 nm in standard BODIPYs [31; 41; 75]. Additionally the emission range of those compounds can be further red-shifted by extending the π-conjugated structure [76; 77]. This suggests that additional efforts to synthesize and understand the impact of atom substitution in this class of dyes are of interest. In a recent work, we have studied the impact of atom exchange directly bonded to the boron atom (OBF_2N *versus* SBF_2N) [78]. While this provided the first example of fluorophores of the BF_2 family with a S-B bond, these molecules were composed of six-membered rings only. In this context, our goal here is to synthesize NMe_2-bearing fluoroborate derivatives containing one five-membered ring and to compare their photophysical properties with their unsubstituted analogues (Scheme 1). One can expect that the impact of atom-exchange is stronger in five-membered ring than in their six-membered counterparts, because of the higher strain in the former compounds. We underline that atom exchange does not influence only the electronic

properties but also impacts the vibrations in the five-membered ring and, in turn, can modify the vibronic couplings and hence the absorption and fluorescence band shapes [79; 80]. In more detail, we have three goals here: i) studying the effect of atom exchange on fluorophores incorporating or not a strong donor group; ii) probing the electron accepting properties of three different five-membered heterocycles; and iii) gaining insights into the electronic structure of the newly synthesized compounds using first principles calculations

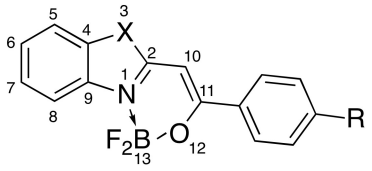

1. X = NMe, R = H
2. X = NMe, R = NMe_2
3. X = O, R = H
4. X = O, R = NMe_2
5. X = S, R = H
6. X = S, R = NMe_2

Scheme 1: The general structure of BF_2-complexes of various heterocycles studied herein.

2. Experimental and theoretical methods

2.1. Experimental methods

The 2-phenacylheterocycles [49; 81] were first obtained and next converted to their BF_2 complexes following the procedure established for similar derivatives [50; 82]. For all presented structures NMR data (^{1}H, ^{11}B, ^{13}C, ^{15}N and ^{19}F) have been obtained (see Experimental Section at the end of this work). The fluorescence yields were determined in chloroform as follows. The fluorescence spectrum of dilute (A $\approx$ 0.1) solutions of the compounds were recorded by excitation at the absorption band maximum of the reference (see Table S3 in the SI). The quantum yield of the tested compounds (Φ_{dye}) was calculated using the following equation [83]:

$$\Phi_{\mathrm{dye}} = \Phi_{\mathrm{ref}} \frac{I_{\mathrm{dye}} A_{\mathrm{ref}}}{I_{\mathrm{ref}} A_{\mathrm{dye}}} \cdot \frac{n_{\mathrm{dye}}^2}{n_{\mathrm{ref}}^2}$$

where Φ_{ref} is the fluorescence yield of the reference, A_{dye} and A_{ref} are the absorbance of the dye and reference samples at the excitation wavelengths, I_{dye} and I_{ref} are the integrated emission intensity for the dyes and references samples, n_{dye} and n_{ref} are the

refractive indices of the solvents used for the dyes and reference, respectively. Knowing the (average) lifetime of the S_1 excited state (τ_{av}) and the fluorescence quantum yield (Φ_{fl}), the radiative (k_r) and nonradiative (k_{nr}) rate constants were calculated using:

$$k_r = \frac{\Phi_{\mathrm{fl}}}{\tau_{\mathrm{av}}}$$

$$k_{nr} = \frac{1 - \Phi_{\mathrm{fl}}}{\tau_{\mathrm{av}}}$$

2.2. Computational details

The geometries of the six studied compounds were optimized in their electronic ground state (GS) at the B3LYP/6-311++G(d,p) level of theory. The effects of the solvent ($CHCl_3$ solution is used consistently with experiment, except when noted) were included by means of the linear-response variant of polarizable continuum model (LR-PCM) [84]. The minimal nature of the optimal GS geometries was confirmed by evaluation of the Hessian. These minimum-energy geometries were used in all subsequent molecular dynamics simulations described below. In order to determine the vertical electronic spectra we have applied the state-of-the-art polarizable-embedded resolution-of-identity second-order coupled-cluster (PERI-CC2) method [85]. In more detail, we firstly carried out molecular dynamics (MD) calculations for BF_2-complexes in chloroform solvent and the trajectories were subjected to subsequent PERI-CC2/MM calculations. During the MD simulations, the interactions between the solute and solvent subsystems were described considering both electrostatic and van der Waals interactions, and this requires charges and force field parameters for each of the molecules. The electrostatic potential fitted charges for the difluoroborates were obtained using the B3LYP/6-311++G(d,p) level of theory and CHEPLG procedure [86] as implemented in Gaussian 09 software. To describe the van der Waals interactions, we employed General AMBER Force Field (GAFF) [87] and CHCL3.frcmod for BF_2-carrying and chloroform solvent molecules, respectively. Selected chloroform force field includes both bond length and bond angle parameters making the solvent flexible. Even though GAFF provides a flexible molecular model

for solutes, we treated the difluoroborates molecules with rigid body approximation. The simulations for BF_2-carrying compounds in chloroform encompassed a single solute molecule and a few thousands of solvent molecules. The calculations were carried out at room temperature and 1 atmospheric pressure using the Amber16 software [88]. The calculations were performed in an isothermal-isobaric ensemble, so that the density of the solute-solvent system evolves to the right value independent of the initial density. The maintenance of the system at a specific temperature and pressure has been achieved by connecting the system to Langevin's thermostat and Barendsen's barostat. The time step for integration of equation of motion was set to 2 fs and the total time scale for the production run was 10 ns. The convergence of key properties (energies and density) in each simulation was checked. Fifty configurations from the last 5 ns simulations selected at equal intervals have been used for computing the spectra using PERI-CC2 method which describes the interaction between the solute-solvent subsystems using electrostatic embedding. The same force-fields as in the MD simulations were used to describe the solvents during the PERI-CC2 calculations. The PERI-CC2 calculations were carried out by using the Turbomole package [89].

Since excited-state (ES) properties, e.g., electronic density changes upon electronic excitation, are not available yet at the PERI-CC2 level, we have employed the Kohn-Sham formulation of time-dependent density functional theory (TD-DFT) for their determination. The DFT and TD-DFT calculations were performed with the Gaussian 09 package [90], employing 11 different exchange-correlation functionals (XCF), i.e., BLYP [91; 92], B3LYP [93], PBE0 [94; 95], M06 [96], BHandHLYP [97], CAM-B3LYP [98], M06-2X [96], ωB97X [99], ωB97X-D [100], LC-BLYP [101], and M06-HF [102; 103]. Five excited states were considered. For all DFT/TD-DFT calculations, we used so-called *ultrafine* integration grid. The density difference plots were simulated with a 0.002 au contour threshold, with density increase (decrease) indicated by red (blue) zones. Subsequent charge-transfer parameters, namely the distance on which charge is transferred (d_{CT}), the amount of charge (q_{CT}) and the dipole moment change upon transition ($\mu_{\mathrm{CT}} = \mu_{\mathrm{ES}} - \mu_{\mathrm{GS}}$)

were calculated using Le Bahers' procedure described in details elsewhere [104; 105]. In this procedure, the CT parameters are determined using the barycenters of density increase and decrease upon photon absorption. All calculations of transition energies were performed with the aug-cc-pVDZ basis set [106–108].

3. Results and discussion

The measured absorption and emission spectra of all six compounds obtained in chloroform are given in Figure 2 and the associated data are listed in Tables 1 and 2. Let us first discuss the results obtained for the absorption spectra. Obviously, the absorption bands of the unsubstituted compounds (R=H) are blue-shifted compared to the R=NMe_2 dyes, a statement holding irrespective of the X heteroatom. Indeed, for all unsubstituted compounds (X=NMe, O, and S) the absorption band peaks at 350–375 nm, whereas for R=NMe_2 the span is twice as large (400–450 nm). In addition, both the shapes and the positions of the absorption bands of the unsubstituted X=NMe and X=O compounds are highly similar, whereas the corresponding NMe_2-substituted derivatives show more pronounced discrepancies in their band topologies. Introducing the donor group also yields a significant evolution of the band shape for the thio derivative.

Table 1: Photophysical properties of examined compounds measured in chloroform.

Struct.		λ_{abs}	λ_{fl}	ε	Δ_{ss}	Φ_{fl}^{a}	Φ_{fl}^{b}
X	R	[nm]	[nm]	[$M^{-1}cm^{-1}$]	[cm^{-1}]	[%]	[%]
NMe	H	349	420	21400	4844	< 1	< 1
O	H	351	424	27000	4905	< 1	< 1
S	H	369	444	26300	4578	1	< 1
NMe	NMe_2	398	443	28000	2552	49	46
O	NMe_2	411	457	42500	2449	98	86
S	NMe_2	447	480	59800	1538	70	68

[a] - quantum yield measured with the use of the references, [b] - quantum yield measured with the use of integrating sphere.

As can be seen in Table 1, the measurements of the fluorescence quantum yields for

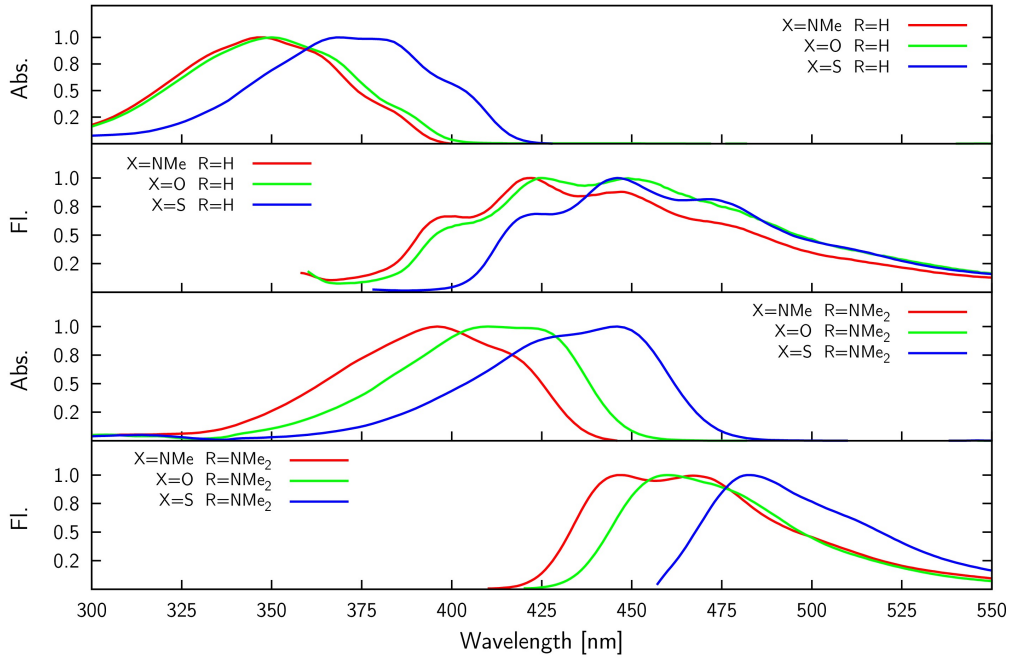

Figure 2: Experimental absorption and emission spectra in $CHCl_3$.

R=NMe_2 dyes returned very high values (Φ_{fl} of 48.7, 98.2, and 70.0% for X=NMe, X=O and X=S respectively) thereby representing huge increases compared to their unsubstituted counterparts (all <1%). Clearly, the enhancement of Φ_{fl} values is also dependent on heteratom type, since in both the R=NMe_2 and R=H series, Φ_{fl} are improved following NMe→O and/or NMe→S substitution. At this stage, we hypothesize that the vibrations and rotations around the single bonds separating the BF_2 scaffold and the side phenyl ring (see Scheme 1) that are likely to quench the emission of the dyes in solution, are significantly limited when an amino group is added. Consistently with the measured quantum yields, enhanced fluorescence lifetimes are observed for the NMe_2 substituted dyes (see Table 2 and the fluorescence decay profiles in Figures S10–S15 in the SI). For the unsubstituted compounds, two exponential fluorescence decays were observed (See Table 2) with a major component close to 70–90 ps and another at ca. 0.9–1.8 ns. In contrast, in the NMe_2 series, the fluorescence decay profiles fit well with

a single-exponential function, giving fluorescence lifetimes of 0.86, 1.59 and 1.78 ns for X=NMe, O, and S, respectively. In other words, in the amino series, the fluorescence lifetimes increase along with the NMe→O→S pattern. From the Table 2 one also notices that the radiative rate constant (k_r) increases when the compounds are substituted by electron releasing substituent NMe_2, i.e., the enhancement of Φ_{fl} originates in both the expected decrease of k_{nr} (*vide supra*) and the increase of k_r. The differences in the k_r values for R=H series are not significant but the k_r/k_{nr} ratio between is two- or three orders lower than unity, indicating that the non-radiative deactivation of S_1 is efficient. The situation is opposite in the R=NMe_2: the k_r/k_{nr} ratio is close to unity for X=NMe derivative and becomes even higher in the X=S and X=O derivatives.

Our next step was to check how solvatochromic effects affect the properties of R=H and R=NMe_2 derivatives, thus we measured absorption and emission properties of the examined dyes in three solvents characterized by different dielectric constant. The electronic absorption and fluorescence spectra recorded in methylcyclohexane (MCH), N,N-dimethylformamide (DMF) and tetrahydrofuran (THF) can be found in Figures S8–S9 in the SI whereas the corresponding spectroscopic and photophysical properties are collected in Tables S5 and S6. As can be seen in Figure S8, the UV-vis absorption spectra of the unsubstituted difluoroborates (R=H) do not display any significant variation of their absorption maxima position, when changing the solvent dielectric constant. In contrast, the absorption maxima of the dimethylamine-substituted derivatives undergo positive solvatochromism, e.g., a noticeable red-shift from 439 nm in MCH to 450 nm in DMF is found for the X=S R=NMe_2 compound (see Figure S9 in the SI). These red-shifts of the absorption maxima position along with the high molar absorption coefficients indicate that the transitions of the R=NMe_2 derivatives have a $\pi - \pi^*$ nature associated with a significant charge transfer (CT) (see Table S5). Similarly, a considerable redshift driven by a solvent dielectric constant change is also observed in the emission spectra of X=O R=NMe_2 and X=S R=NMe_2 compounds, whereas no significant shift was found in the fluorescence spectra of unsubstituted difluoroborates, indicating that the

CT character of the first singlet excited state is much more marked in the dimethylamine derivatives [109; 110]. Interestingly, the emission spectra of the X=NMe R=NMe_2 dye display significantly smaller solvatochromic shifts, than their benzoxazole and benzothiazole analogues. In short, the redshifts of the emission maxima positions, as well as higher sensitivity of fluorescence spectra (with respect to absorption) to the dielectric constant of the environment are characteristics of push-pull compounds undergoing CT transitions [109–112].

As can be seen in Table S5, the fluorescence quantum yields of the unsubstituted dyes remain very small (<1%), irrespective of the solvent dielectric constant. Obviously, such trifling values do not allow for an unambiguous interpretation of the impact of the solvent dielectric constant on the Φ_{fl}; the trends being however similar as in $CHCl_3$. In contrast, the R=NMe_2 dyes fluoresce intensively in all studied solvents. The Φ_{fl} of the X=S R=NMe_2 compound is systematically decreasing with increasing solvent dielectric constant, which is a usual trend in dyes exhibiting large charge separation in their excited state [113; 114]. Interestingly, the opposite is observed for X=NMe R=NMe_2 dye, in which fluorescence quantum yield increases from 14.5% (MCH) up to 56.5% (DMF). It is not easy to interpret this peculiar behavior but we hypothesize that it is related to the motion of the additional methyl group that would be somehow diminished in DMF. Indeed, such improvement of the fluorescence quantum yield with increasing in solvent dielectric constant, also known as negative solvatokinetic effect, might be connected with interactions between the excited solute and solvent molecules, which changes the excited-state configuration and the fluorescence intensity [115–120]. However, the above hypothesis needs more precise studies in a wider range of solvents and is out of the scope of the current work. Eventually, for X=O R=NMe_2, the Φ_{fl} is similar in THF (68.9%) than in MCH (73.5%), but a lower efficiency is observed in the most polar DMF (52.5%) , as usual. We also highlight that, irrespective of the selected solvent, the unsubstituted compounds exhibit a two-exponential decay emission whereas the R=NMe_2 dyes show mono-exponential decays, but for X=NMe R=NMe_2 in MCH.

Table 2: Fluorescence lifetimes (τ), component amplitudes (α), correlation coefficients (χ^2) and radiative (k_r) and non-radiative (k_{nr}) rate constants for examined compounds in chloroform.

Struct.		τ_1	τ_2	α_1	α_2	τ_{av}	χ^2	k_r	k_{nr}	k_r/k_{nr}
X	R	[ps]	[ps]			[ps]		$[\text{s}^{-1}] \times 10^8$	$[\text{s}^{-1}] \times 10^8$	
NMe	H	72	1630	99.345	0.654	82.2	1.668	0.29	121	0.0024
O	H	71	1981	98.785	1.215	94.2	1.439	0.33	106	0.0031
S	H	86	1021	99.438	0.562	91.3	1.538	1.32	108	0.0120
NMe	NMe_2	-	861	-	100	861	1.395	5.66	5.96	0.95
O	NMe_2	-	1593	-	100	1593	1.077	6.16	0.12	53.6
S	NMe_2	-	1775	-	100	1775	1.172	3.94	1.69	2.33

The fluorescence excitation and emission characteristics of all compounds have been measured in THF at different emission and excitation wavelengths. As can be seen in Figures S4 and S5 in the SI, the position of the fluorescence peaks remains constant independently of both the λ_{exc} and concentration in the solution for all compounds. This clearly suggests at a rapid internal conversion from higher excited states to the lowest vibrational energy level of the S_1 state as well as the presence of only one emitting species. In addition, the fluorescence excitation spectra were recorded for two emission wavelengths (detection at blue and red edges of the emission spectrum), as well as at the maximum of the emission spectrum for diluted and more concentrated solutions. Figures S6 and S7 display the steady-state fluorescence excitation spectra of the tested compounds, and one can observe, on the one hand, spectra independent of the considered wavelength, and, on the other hand, a non-negligible impact of the concentration of the solution. The differences between absorption and excitation spectra of the dyes in 10^{-5} M solutions show the existence of the excited molecules that differ in spatial conformations and/or solvent relaxations.

All these experimental results encouraged us to carry out computer simulations in order to shed light onto the electronic structure of these derivatives, one of our goals being to unravel the origin of the band shape differences: multiple electronic state and/or various vibronic couplings. Our results are presented in Table 3. As can be seen, the

first electronic excited state is well separated from the second one, with an energy gap between them attaining ca. 1 eV for all studied molecules. In addition, the oscillator strengths, f are much larger for the $S_0 \rightarrow S_1$ transition (from 1.07 to 1.59) than for the $S_0 \rightarrow S_2$ transition (from 0.02 to 0.06). This clearly indicates that the observed spectra are solely due to the first electronic ES. For that excitation, the NMe_2-substituted compounds exhibit larger oscillator strengths than their unsubstituted counterparts. We note that the predicted f values are rather consistent with measured molar absorptivities (see ε in Table 1): in both cases, significantly lower values are obtained for R=H derivatives. Nevertheless, based on the measurements, one would have expected significantly lower oscillator strength for the X=NMe R=NMe_2 derivative. Figure 3 shows the simulated vertical absorption spectra in the 300–550 nm range, considering the absorption bands of the $S_0 \rightarrow S_1$ transition. As discussed above, the PERI-CC2 calculations were performed based on 50 solute-solvent configurations (for each compound) considering rigid dyes and flexible chloroform molecules. Therefore, the widths of the absorption bands shown in Figure 3 originate from the inhomogeneous broadening due to solute-solvent interactions, whereas the vibronic couplings are neglected, so that the band widths are logically underestimated compared to experiment. Nevertheless, by comparing the R=H and R=NMe_2 derivatives, one clearly notices that the latter are much more sensitive to the solvent microenvironment, explaining the larger inhomogeneous broadening of derivatives possessing a dimethylamino group (see the σ values in Table 3), a feature that can be directly associated with an increase of the intramolecular charge-transfer character when adding the electron-donating group. As neither the presence of multiple electronic states nor explicit solvent-solute interactions can explain the presence of several maxima/shoulders in the absorption spectra of Figure 2, these band shapes should reflect the changes in the vibrational fine structure induced by chemical modifications. To confirm this hypothesis, complementary calculations were performed using CC2 method, but in gas phase (see Figure S3 in the SI). Although these calculations do not account for the solvent environment, and hence, logically yield band positions that are blue-shifted compared to the

measurements and PERI-CC2 results, one notices that the experimental band shapes are reasonably well reproduced, confirming the vibronic nature of the multi-peak absorption bands.

Table 3: Average vertical excitation energies ($\Delta\overline{E}$), standard deviations of ΔE distributions ($\sigma(\Delta E)^*$) and average oscillator strengths ($\overline{f}$) computed at the PERI-CC2/aug-cc-pVDZ level of theory in chloroform. *FWHM=$2\sqrt{2\ln\sigma(\Delta E)}$.

Struct.		$\Delta\overline{E}$ [eV]	$\Delta\overline{E}$ [nm]	$\sigma(\Delta E)$ [eV]	$\overline{f}$
X	R		$S_0 \rightarrow S_1$		
NMe	H	3.73	333	0.01	1.12
O	H	3.70	335	0.01	1.12
S	H	3.44	361	0.01	1.07
NMe	NMe_2	3.19	389	0.05	1.59
O	NMe_2	3.07	404	0.05	1.59
S	NMe_2	2.90	428	0.06	1.57
			$S_0 \rightarrow S_2$		
NMe	H	4.73	262	0.02	0.02
O	H	4.66	266	0.04	0.02
S	H	4.42	280	0.05	0.05
NMe	NMe_2	4.19	296	0.03	0.06
O	NMe_2	4.20	295	0.02	0.06
S	NMe_2	4.00	310	0.02	0.03

Let us now assess the accuracy of the PERI-CC2 method in reproducing the auxochromic shifts on the absorption spectra. In Table 4 the experimental and simulated spectral shifts of the $S_0 \rightarrow S_1$ absorption band maxima are listed. In that Table, we used the X=NMe R=H compound as a reference. The experimentally determined shift upon X=NMe→O replacement is trifling for R=H (+2 nm) but significant for R=NMe_2 (+14 nm). The respective shifts predicted by the PERI-CC2 method are +3 nm and +15 nm, thus demonstrating the excellent agreement with experimental data. Significantly larger auxochromic effects are observed experimentally for the X=NMe→S substitution, i.e., +20 nm for R=H and +50 nm for R=NMe_2, with again simulated shifts in good agreement (+28 nm and +40 nm). One can therefore conclude that the overall

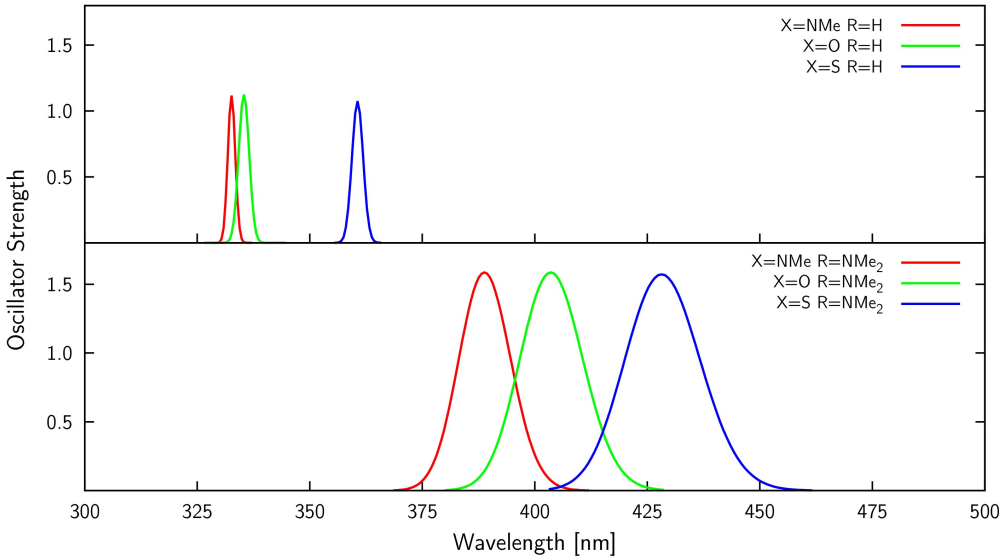

Figure 3: Electronic vertical absorption spectra simulated at the PERI-CC2/aug-cc-pVDZ level of theory.

agreement between the PERI-CC2 simulation results and the experimental data is, at the very least, satisfactory, thus further consolidating the above conclusions regarding the origin of the specific band shapes.

In order to obtain additional insights into the electronic structure of the dyes, we have probed the nature of the excited state properties in the Franck-Condon region. Since ES properties cannot yet be determined with the PERI-CC2 approach, we have turned towards TD-DFT. The performance of TD-DFT in predicting ES properties is known to significantly depend on the selected XCF [121; 122], and no single XCF can be considered as outperforming the others on a systematic basis. Hence, in order to select a XCF providing accurate results for the molecules under investigation, we have benchmarked eleven XCFs and compared the obtained GS and ES dipole moments to CC2 reference values. The dipoles were chosen as they are a measure of the quality of the electronic density and are also directly related to the CT character of the electronic transition. These benchmark calculations were performed for isolated (no solvent) molecules. As can be seen in Figure 4, the errors made by DFT for GS dipole moments (μ_{GS}) are sub-

Table 4: Excitation energy changes, w.r.t. X=NMe R=H compound, induced by chemical modifications: comparisons between theory (PERI-CC2 and PCM-TD-B3LYP) and experiment.

Struct.		$S_0 \rightarrow S_1$					
X	R	exp.	exp.	PERI-CC2	PERI-CC2	PCM-TD-B3LYP	PCM-TD-B3LYP
		[eV]	[nm]	[eV]	[nm]	[eV]	[nm]
NMe	H	0.00	0	0.00	0	0.00	0
O	H	-0.02	+2	-0.03	+3	0.00	0
S	H	-0.19	+20	-0.29	+28	-0.17	+18
NMe	NMe_2	-0.43	+48	-0.54	+56	-0.37	+43
O	NMe_2	-0.54	+62	-0.66	+71	-0.42	+50
S	NMe_2	-0.78	+98	-0.83	+96	-0.57	+70

stantially smaller compared to the TD-DFT errors for the ES (μ_{ES}), which is consistent with previous benchmarks [123; 124]. As a consequence, the errors in the so-called excess dipole moments (μ_{GS}-μ_{ES}) are mainly originating from the TD-DFT part. For the μ_{GS} the smallest errors are reached with the ωB97X XCF (smaller than 0.2 D), although all XCFs provide satisfying results. In contrast, for the ES, ωB97X yields the largest maximum deviations (ca. 3.0 D), whereas B3LYP provides the smallest maximum error for both μ_{ES} (1.3 D) and μ_{ES}-μ_{GS} (1.9 D). B3LYP also gives one of the smallest average errors for μ_{GS} (0.3 D), μ_{ES} (1.2 D), and μ_{ES}-μ_{GS} (1.3 D). In addition, this XCF accurately reproduces the impact of chemical substitution on the ES dipoles, but for a slight underestimation of the dipole increase when adding the dimethylamino group. Therefore we select B3LYP for our analysis of the ES properties in $CHCl_3$ solution. As can be seen in Table 4, PCM-TD-B3LYP also fairly reproduces all auxochromic shifts though less accurately than with PERI-CC2, as expected. We are well aware of the inherent limits of B3LYP for describing long-range CT systems [122], but the molecules considered are probably compact enough so that these limits are not relevant here.

Table 5 provides a summary of the TD-DFT ES properties computed in the Franck-Condon region together with electron density difference (EDD) plots showing the electronic reorganization accompanying the transition to the lowest electronic excited state.

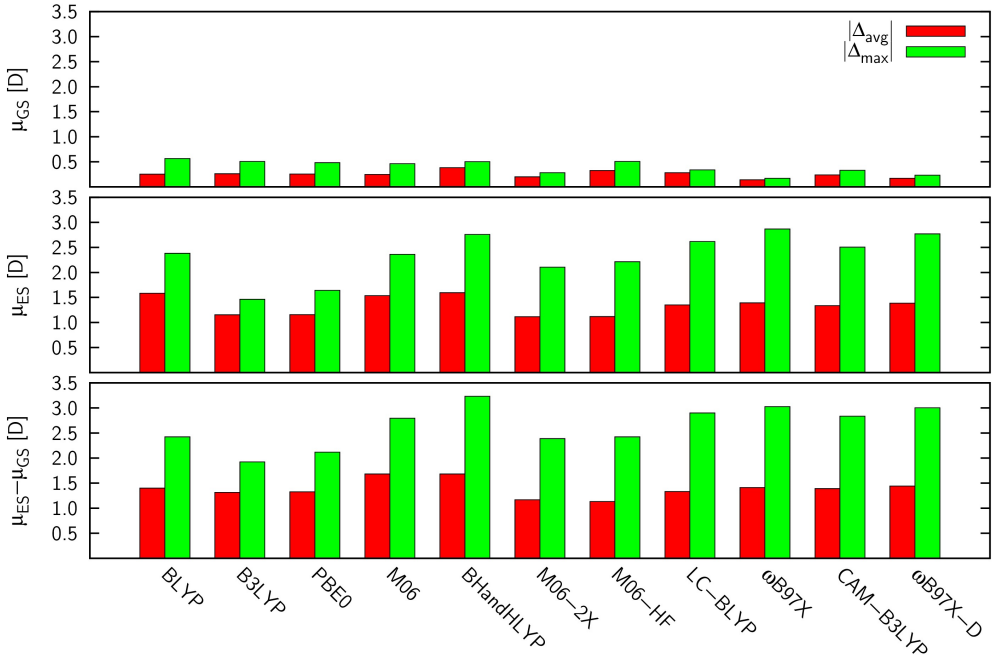

Figure 4: Errors in TD-DFT dipole moments: maximum (Δ_{max}) and average (Δ_{avg}) absolute errors compared to CC2 (see also corresponding Table S1 in the SI). All results were obtained in gas phase with the *aug*-cc-pVDZ basis set.

As can be seen, for the R=H compounds, the electronic density changes mainly take place within the BF_2-containing core and adjacent five-membered ring. In contrast for molecules bearing a NMe_2 group, the density changes involve not only the BF_2-carrying ring but also the side NMe_2-phenyl moiety, the amino group acting, as expected, as a donor (mostly in blue in the EDDs). The CT character of the transitions in NMe_2 derivatives is reflected by the significant values of the dipole moment differences (μ_{ES} - μ_{GS}) which exceed 6 D for all three dyes, whereas significantly smaller values are obtained for the R=H derivatives. Logically, the charge-transfer distances d_{CT} are increasing upon NMe_2 substitution (up to $d_{\mathrm{CT}} \approx 2.7$ Å). However as one can see the d_{CT} values of X=NMe R=H ($d_{\mathrm{CT}} = 2.310$ Å) and X=O R=H ($d_{\mathrm{CT}} = 2.110$ Å) derivatives are much closer to their NMe_2-substituted counterparts, than to X=S R=H ($d_{\mathrm{CT}} = 1.539$ Å). This can be explained by looking at the EED of R=H derivatives collected in Table 5, as one

can see both X=O and X=NMe derivatives have red (accepting) lobes on the bond connecting the fluoroborate core to the adjecent phenyl ring. This indicates that d_{CT} in fact should be larger for those two derivatives. Additionally, the R=NMe_2 compounds are also characterized by a larger transferred charge (q_{CT} of ca. 0.50 e) than in their R=H counterparts (q_{CT} in the 0.41–0.43 e range). In the R=H series the CT character of the electronic transition is clearly decreasing following X=NMe→O→S, which is confirmed by a systematic decrease of both the d_{CT} (NMe→O=-0.209 Å, O→S=-0.562 Å) and μ_{ES}-μ_{GS} (NMe→O=-0.395 D, O→S=-1.332 D) parameters. An interesting observation can be made by comparing NMe_2-substituted compounds, i.e., d_{CT} and μ_{ES}-μ_{GS} values are lowest for X=O (d_{CT}=2.713 Å, μ_{ES}-μ_{GS}=6.537 D), while opposite to R=H, the highest values are obtained for the thio derivatives (d_{CT}=2.751 Å, μ_{ES}-μ_{GS}=6.612 D). In turn X=NMe d_{CT} values are close to X=O, whereas μ_{ES}-μ_{GS} results are similar to those of X=S. Comparing the parameters of Table 5 to the fluorescence quantum yields, one notices that the decrease of the d_{CT} and μ_{ES}-μ_{GS} promotes the radiative transition for all three dyes of each series (R=H and R=NMe_2), e.g., in the R=H series the quantum yield decreases with increasing CT character. In contrast, Φ_{fl} is much higher in the NMe_2 series, although the CT character is enhanced in the latter. We hypothesize that this result comes from the fact that in the amino dyes, the CT involves the electron lone pair of the amino nitrogen, which allows the formation of a quinoidal structure, and hence lead to the rigidification of the excited state. That conclusion is also supported by the single-exponential fit of the fluorescence decay (see Figures S10–S15 in the SI).

To further ascertain the CT character of the amino-substituted dyes, we calculated the excited-state properties in Franck-Condon region of the benzothiazole derivatives in three additional solvents: MCH, DMF and THF. The results of those calculations together with the corresponding EDD plots are presented in Table S3 in the SI. As can be seen, the above-described trends (obtained in chloroform) pertain, e.g., the S_0→S_1 transition is associated with a much smaller μ_{ES}-μ_{GS} in the R=H (not exceeding 3 D) than in the R=NMe_2 dye (larger than 5.8 D). The EDD plots also tend to confirm the

Table 5: Electron density difference plots and related electron transition parameters. All results were obtained at B3LYP/aug-cc-pVDZ level of theory for chloroform solution. Blue (red) color marks electron density depletion (gain) upon photon absorption. The contour value was set to 0.002 au.

Struct.		EDD plots	d_{CT}	q_{CT}	$\mu_{ES} - \mu_{GS}$
X	R		[Å]	[e]	[D]
NMe	H	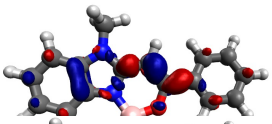	2.310	0.427	4.734
O	H		2.101	0.430	4.339
S	H		1.539	0.407	3.007
NMe	NMe_2	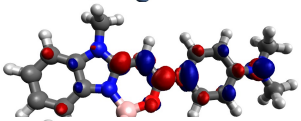	2.725	0.504	6.595
O	NMe_2	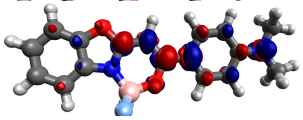	2.713	0.502	6.537
S	NMe_2	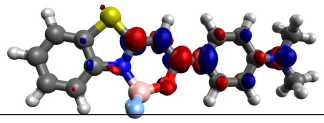	2.751	0.500	6.612

CT nature of $S_0 \rightarrow S_1$ transition of the R=NMe_2 derivatives: with density variations in the R=NMe_2 derivative showing a clear CT from the *p*-NMe_2-phenyl moiety (donor) to the BF_2-bearing moiety (acceptor).

To further characterize the first excited state beyond the Franck-Condon region, we have optimized the excited-state geometries of all compounds using TD-DFT. Let us first discuss the changes in bond lengths between the two electronic states. The complete set of data can be found in Table S2 in the SI. We focus our analysis on the geometrical changes, as given by $\Delta^{EG}_{bond} = bond^{ES} - bond^{GS}$. A graphical representation of the general variations of geometries can be found in Scheme 2. First, based on the comparison of

the sum of absolute changes of bond lengths in the series, it appears that the $S_0 \rightarrow S_1$ excitation induces stronger effects for unsubstituted derivatives (R=H) than that for their substituted analogues (R=NMe_2). Indeed, the total variations, $\Sigma\Delta^{EG}_{bond}$, are equal to 1.249 Å and 1.157 Å, for the R=H and R=NMe_2 series, respectively. This holds for the bonds belonging to the heterocyclic part of the structures, confirming that the excitation causes more dramatic changes in geometry for R=H, which is detrimental for emission yields. In contrast, except for the C11-C14 distance, the opposite trends are observed for 1,4-phenylene ring moieties. This can be easily explained by the presence of NMe_2 donor which strongly affects the electron density distribution thus also the geometry of the R=NMe_2 dyes (See Figure S2 in the SI). Second, most of the computed changes in bond distances follow a N→O→S ranking, e.g., for the C10-C11 bond, the excitation-induced changes are maximal for X=S derivatives and minimal for their X=NMe counterparts. In contrast, for the C9-N1 bond distance the above trend is reversed in both dye series (See Figure S1 in the SI). Third, for the side phenyl rings, the expected *p*-quinoid form (=(C(-CH=CH-)$_2$C)=) is favored upon excitation. This can be deduced based on the fact that two, out of six, ring bonds are shorter, while four of them are elongated when passing from the GS to the ES geometry (see Scheme 2). Interestingly, somewhat similar trends are observed for five-membered ring, i.e., N1-C2 and C2-X3 bonds become longer, while X3-C4 and C9-N1 distances become shorter upon excitation.

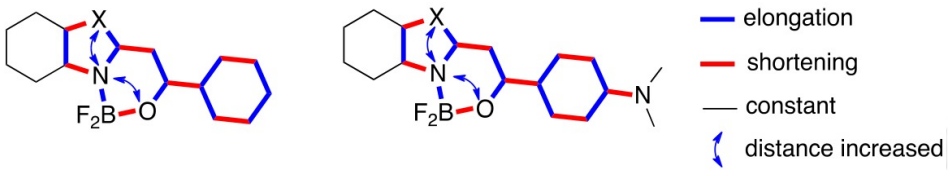

Scheme 2: Schematic representation of geometry changes upon excitation in R=H and R=NMe_2 dyes.

4. Conclusions

We have investigated the influence of heteroatom (X=O, S, and NMe) substitution in five-membered heterocyclic ring on the photophysical properties of novel BF_2 complexes containing or not a dimethylamino group (R=NMe_2). The experimental results showed that the photophysical properties of the molecules bearing an electron-donating group are substantially different from these observed for unsubstituted analogues, which follows previous findings of our groups [2; 50; 82]. For instance, the NMe→O heteroatom replacement has a negligible impact on the absorption and emission properties of R=H derivatives, but induces significant red-shifts accompanied by changes of the relative intensities of absorption/emission shoulders for R=NMe_2 compounds. More pronounced changes stem from the NMe→S substitution, i.e., both R=H and R=NMe_2 optical bands are substantially redshifted. It is noteworthy that all R=NMe_2 derivatives exhibit fluorescence quantum yields significantly higher (up to one order of magnitude) than their unsubstituted counterparts. The experimental data were supported by the quantum chemistry calculations, which not only reproduced the experimental trends but also contributed to the understanding of electronic structure and excited-state properties: i) the different photophysical properties of the R=NMe_2 fluorophores likely result from the more pronounced CT character of their $S_0 \rightarrow S_1$ transition, as evidenced by both the large inhomogeneous broadening of the absorption spectra obtained with the PERI-CC2 simulations and the dipole moment differences obtained at various levels of theories; ii) the difference between absorption band topologies of R=H and R=NMe_2 have their roots in the CT nature of the latter derivatives, that washes out the impact of vibronic couplings, as PERI-CC2 calculations show that only one electronic state contributes to the overall visible absorption band; and iii) the enhancement of fluorescence quantum yield observed for compounds with R=NMe_2 can be linked to stabilization of a more planar structure, both in the ground and the excited electronic states.

5. Experimental Section

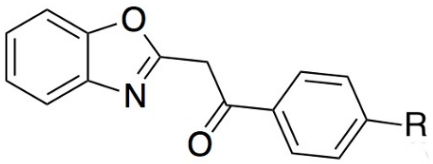

R = NMe_2, H

In general, 2-phenacylbenzoxazoles can be obtained in the condensation of 2-aminophenol and 3,3-dialkoxy-3,3-dimercapto-1-phenylprop-2-en-1-ones [125; 126] or alkyl benzoylacetates [127]. These compounds were also conveniently prepared by subtraction of one of the methyl protons in 2-methylbenzoxazole and treatment of the formed carbanion with acylating agent such as benzoic acid ester or benzoyl chloride [81; 128–137]. All compounds discussed in the present paper were obtained in the two-step synthesis starting from 2-methylbenzoxazole and substituted benzoyl chlorides as before [133]. It is worth underscoring the tautomeric equilibrium exists in these compounds.

2-Phenacylbenzoxazole - White solid, yield 59%, Mp 94–96°C; 94–96°C [81], 88–88.5°C [126], 88–88.5°C [128], 88°C [129], 90–91°C [130], 97–98°C [125], and 93.5–94.5°C [131]. In $CDCl_3$ solution 2-phenacylbenzoxazole (ketimine tautomeric form) is in equilibrium with (Z)-2-(1,3-benzoxazol-2-yl)-1-phenylethenol (enolimine form). ^{1}H NMR ($CDCl_3$ from TMS) δ: 12.50 (br s, 1H), 8.06 (m, 1H), 7.89 (m, 3H), 7.73 (m, 1H), 7.62 (m, 2H), 7.50 (m, 3H), 7.46 (m, 4H), 7.33 (m, 2H), 7.29 (m, 1H), 6.21 (s, 1H), 4.64 (s, 1H). ^{13}C NMR δ: 192.4, 166.3, 165.74, 160.4, 151.3, 148.8, 141.3, 139.9, 135.8, 134.1, 133.9, 130.6, 128.9, 128.6, 128.6, 125.9, 125.0, 124.6, 124.3, 124.1, 120.0, 117.9, 110.6, 110.2, 83.7, 39.6. ^{15}N NMR ($CDCl_3$ from $MeNO_2$) δ: -134.4, -164.1. $C_{15}H_{11}NO_2$ Calcd. C 75.94, H 4.67, N 5.90; Found C 75.87, H 4.75, N 5.83.

2-(1,3-benzoxazol-2-yl)-1-[4-(dimethylamino)phenyl]ethanone - White solid, yield: 73%, Mp 199–200.4°C; 197–198°C [81]. In $CDCl_3$ solution 2-(1,3-benzoxazol-2-yl)-1-[4-(dimethylamino)phenyl]ethanone (ketimine tautomeric form) is in equilibrium with (Z)-2-(1,3-

benzoxazol-2-yl)-1-[4-(dimethylamino)phenyl]ethenol (enolimine form). ^{1}H NMR ($CDCl_3$ from TMS) δ: 7.96 (m, 2H), 7.72 (m, 1H), 7.50 (m, 1H), 7.29 (m, 2H), 6.68 (m, 2H), 6.05 (s, 1H, signal of low intensity coming from low amount of the enolimine form), 4,53 (s, 1H), 3.05 (s, 6H). ^{13}C NMR δ: 190.0, 166.7, 161.6, 153.9, 151.3, 141.5, 131.0, 127.3, 124.8, 124.4, 124.2, 123.7, 123.4, 119.9, 111.5, 110.8, 110.6, 80.4, 40.0, 39.1, ^{15}N NMR ($CDCl_3$ from $MeNO_2$) δ: -135.6, -322.9. $C_{17}H_{16}N_2O_2$, Calcd. C 72.84, H 5.75, N 9.99. Found C 72.66, H 5.88, N 9.86.

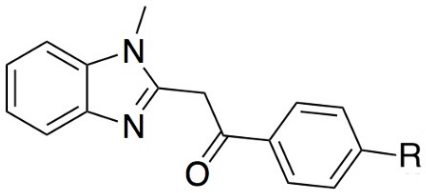

R = NMe_2, H

Some of 1-methyl-2-phenacylbenzimidazoles were synthesized according to reaction of benzoyl substituted mercaptals with *N*-methyl-*o*-phenylenediamine [138; 139]. Aforementioned synthesis, as well as other earlier described in the literature [125; 140], are characterized by low yield, therefore 1-methyl-2-phenacylbenzimidazole were prepared by treating 1,2-dimethylbenzimidazole with benzoyl chloride in the presence of triethylamine followed by thermal decomposition of formed 2-(1-methyl-1*H*-benzo[*d*]imidazol-2-yl)-1-phenylvinyl benzoate. Thus, benzoyl chloride (8 mmol) was added at once to the mixture of 1,2-dimethylbenzimidazole (0.29 g, 2 mmol), triethylamine (0.81 g, 8 mmol) and diglyme (10 mL) and the resulted mixture was heated (steam bath) and stirred overnight. Addition of water (6 mL) precipitated the byproduct. Solution of morpholine (0.52 g, 6 mmol) in methanol (3 mL) was added to crude 2-(1-methyl-1*H*-benzo[*d*]imidazol-2-yl)-1-phenylvinyl benzoate and the resulted mixture was refluxed for 5 min. Reaction was quenched by addition of water (3 mL) and the precipitated solid product was recrystallized from ethanol.

1-Methyl-2-phenacylbenzimidazole - Yellow solid, yield 40%, Mp 134–135.5°C; 119–

121°C (plates) and 149–152°C (needles) [49], 150–151°C and 134–134.5°C [139], 150–152°C [125; 140], and 150–151.5°C [128; 141]. In $CDCl_3$ solution 1-methyl-2-phenacylbenzimidazole (ketimine tautomeric form) is in equilibrium with (Z)-2-(1-methyl-1*H*-benzimidazol-2-yl)-1-phenylethenol (enolimine form). ^{1}H NMR ($CDCl_3$ from TMS) δ: 14.04 (br s, 1H), 8.13 (d, 2H, $^3J_{H,H}$=7.32 Hz), 7.93 (m, 2H), 7.74 (m, 1H), 7.61 (m, 1H), 7.50 (m, 2H), 7.43 (m, 4H), 7.33 (m, 1H), 7.28 (m, 1H), 7.23 (m, 3H), 5.91 (s, 1H), 4.70 (s, 2H), 3.76 (s, 3H), 3.67 (s, 3H). ^{13}C NMR δ: 194.0, 174.8, 154.4, 148.6, 138.4, 134.9, 134.8, 134.0, 133.14, 130.11, 129.9, 128.93, 128.87, 128.83, 128.3, 127.3, 126.2, 124.3, 122.9, 122.8, 122.7, 122.3, 122.2, 119.3, 113.9, 110.6, 109.4, 108.3, 77.0, 39.1, 30.5, 29.1. ^{15}N NMR ($CDCl_3$ from $MeNO_2$) δ: -137.4, -210.4, -233.3, -253.5. $C_{16}H_{14}N_2O$, Calcd. C 76.78, H 5.64, N 11,19. Found C 76.85, H 5.74, N 11.03.

A slightly modified procedure [139] was used to prepare 1-[4-(dimethylamino)phenyl]-2-(1-methyl-1*H*-benzimidazol-2-yl)ethanone. A mixture of 1,2-dimethylbenzimidazole (0.29 g, 2 mmol), ethyl 4-(dimethylamino)benzoate (0.39 g, 2 mmol), dry benzene (10 mL), dimethylformamide (0.5 mL) and sodium hydride (0.15 g, 60% suspension in mineral oil) was refluxed and stirred magnetically overnight. The reaction was quenched by addition of water (15 mL) and the resulted mixture was extracted with ethyl acetate (20 mL). The organic layer was subsequently washed with water (2 x 10 mL) and brine (2 x 10 mL) and dried with sodium sulfate. Solid impurities were filtered off, the filtrate was concentrated on the rotary evaporator. The obtained solid was recrystallized from ethanol.

1-[4-(dimethylamino)phenyl]-2-(1-methyl-1*H*-benzimidazol-2-yl)ethanone - Yellow solid, yield 36%, Mp 228–230°C, and 228–230°C [49]. In $CDCl_3$ solution 1-[4-(dimethylamino)-phenyl]-2-(1-methyl-1*H*-benzimidazol-2-yl)ethanone (ketimine tautomeric form) is in equilibrium with (Z)-1-[4-(dimethylamino)phenyl]-2-(1-methyl-1*H*-benzimidazol-2-yl)ethenol (enolimine form). ^{1}H NMR ($CDCl_3$ from TMS) δ: 8.02 (m, 2H), 7.68 (d, 1H, $^3J_{H,H}$=8.80 Hz), 7.74 (m, 2H), 7.30 (m, 1H), 7.24 (m, 1H), 7.18 (m, 2H), 6.73 (m, 4H), 6.66 (m, 2H), 5.81 (s, 1H), 4.61 (s, 2H), 3.78 (s, 6H), 3.03 (s, 6H), 3.01 (s, 6H). ^{13}C NMR δ: 191.7, 170.8, 153.8, 153.5, 149.8, 142.2, 136.1, 131.9, 131.2, 127.5, 123.7, 122.4, 122.3, 122.0, 119.2,

116.8, 111.4, 110.73, 110.67, 110.4, 109.3, 74.9, 40.1, 40.0, 38.8, 30.5. ^{15}N NMR ($CDCl_3$ from $MeNO_2$) δ: -136.8, -233.8, -317.3. $C_{18}H_{19}N_3O$, Calcd. C 73.69, H 6.53, N 14.32. Found C 73.78, H 6.63, N 14.23.

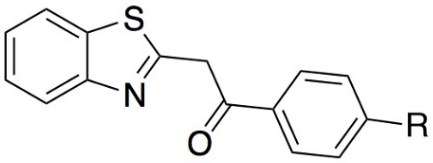

R = NMe_2, H

2-Methylbenzothiazole (2.5 g, 16.7 mmol) was added to a suspension of NaH (2 g, 50 mmol, 60% suspension in oil) in dry THF (15 mL) stirred at room temperature for 2 h. After that time methyl benzoate (3.27 g, 21.8 mmol) or ethyl 4-(dimethylamino)benzoate (4.21 g, 21.8 mmol) was added, and the resulting mixture was heated at reflux and stirred magnetically overnight. After cooling down to room temperature, 2 M HCl aq. was slowly added, and the yellow precipitate was filtered and washed with water. Resulting solid was purified by column chromatography (SiO_2, DMC) [142–144]. Other methods of synthesis of 2-phenacylbenzothiazoles are reported in the literature [125; 128; 134; 136; 137; 145–147].

2-phenacylbenzothiazole - yellow solid, yield 69%, Mp 110.5–112.5°C, 113.5–114.5°C [134], 110°C [129], 114°C [125], 113–114°C [126], 110–111°C [128], and 116–117°C [142]. In $CDCl_3$ solution 2-phenacylbenzothiazole (ketimine tautomeric form) is in equilibrium with (Z)-2-(1,3-benzothiazol-2-yl)-1-phenylethenol (enolimine form). ^{1}H NMR ($CDCl_3$ from TMS) δ: 13.81 (br s, 1H), 8.09 (d, 2H, $^3J_{H,H}$=7.36 Hz), 8.03 (m, 1H), 7.88 (m, 2H), 7.80 (m, 2H), 7.59 (m, 4H), 7.52 (m, 4H), 7.39 (m, 1H), 7.30 (m, 1H), 6.38 (s, 1H), 4.85 (s, 1H). ^{13}C NMR δ: 194.0, 168.1, 165.6, 163.8, 152.3, 150.4, 135.8, 135.2, 134.8, 133.9, 131.4, 130.4, 130.0, 129.1, 128.9, 128.7, 128.5, 127.5, 126.5, 126.2, 125.9, 125.2, 124.2, 122.8, 122.4, 121.6, 121.4, 120.0, 90.9, 43.7. ^{15}N NMR ($CDCl_3$ from $MeNO_2$) δ: -120.0. $C_{15}H_{11}NOS$, Calcd. C 71.12, H 4.38, N 5.53. Found C 71.20, H 4.51, N 5.42.

2-(1,3-benzothiazol-2-yl)-1-[4-(dimethylamino)phenyl]ethanone - yellow solid, yield 77%, Mp 207–208°C. ^{1}H NMR ($CDCl_3$ from TMS) δ: 7.99 (m, 3H), 7.86 (d, 1H, $^{3}J_{H,H}$=8.0 Hz), 7.45 (m, 1H), 7.36 (m, 1H), 6.67 (d, 2H, $^{3}J_{H,H}$=8.0 Hz), 4.75 (s, 2H), 3.07 (s, 6H). ^{13}C NMR δ: 191.8, 165.1, 153.8, 152.6, 136.0, 131.1, 127.5, 126.3, 125.8, 124.9, 123.6, 123.6, 122.7, 121.5, 121.3, 110.8, 88.4, 43.3, 40.0. ^{15}N NMR ($CDCl_3$ from $MeNO_2$) δ: -67.8, -317.1. $C_{17}H_{16}N_2OS$, Calcd. C 68.89, H 5.44, N 9.45. Found C 68.95, H 5.57, N 9.29. The complexes were prepared based on a literature protocol [82]. For

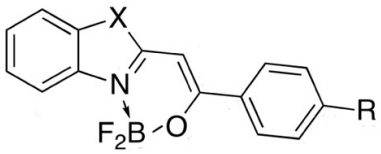

X = O, NCH_3, S R = NMe_2, H

their purification DCM was used as eluent in column chromatography (SiO_2).

1,1-difluoro-5-methyl-3-phenyl-1,5-dihydrobenzo[4,5]imidazo[1,2-*c*][1,3,2]oxazaborinin-10-ium-1-uide (**X=NMe, R=H**) - White solid, yield 36%, Mp 255.6–256.7°C. ^{1}H NMR (DMSO-d_6 from TMS) δ: 8.09 (m, 2H), 7.77 (m, 1H), 7.68 (m, 1H) 7.56 (m, 3H), 7.44 (m, 2H), 7.05 (s, 1H), 3.98 (s, 3H). ^{11}B NMR (DMSO-d_6 from $BF_3{\cdot}Et_2O$) δ: 1.66 (t). ^{13}C NMR δ: 164.8, 150.4, 134.4, 133.8, 132.0, 131.7, 129.2, 126.9, 125.1, 124.8, 114.3, 111.8, 81.8, 30.5. ^{15}N NMR (DMSO-d_6 from $MeNO_2$) δ: -218.76, -242.04. ^{19}F NMR (DMSO-d_6 from $CFCl_3$) δ: -134.14. $C_{16}H_{13}BF_2N_2O$, Calcd. C 64.47, H 4.40, N 9.40; Found C 64.53, H 4.46, N 9.48.

3-(4-(dimethylamino)phenyl)-1,1-difluoro-5-methyl-1,5-dihydrobenzo[4,5]imidazo[1,2-*c*][1,3,2]oxazaborinin-10-ium-1-uide (**X=NMe, R=NMe_2**) - Yellow solid, yield 39%, Mp 282–283.4°C. ^{1}H NMR (DMSO-d_6 from TMS) δ: 7.97 (d, 2H, $^{3}J_{H,H}$=9.04 Hz), 7.74 (m, 1H), 7.65 (m, 1H) 7.46 (m, 2H), 6.85 (d, 2H, $^{3}J_{H,H}$=9.12 Hz), 6.79 (s, 1H), 3.96 (s, 3H), 3.09 (s, 6H). ^{11}B NMR (DMSO-d_6 from $BF_3{\cdot}Et_2O$) δ: 1.59 (t). ^{13}C NMR δ: 166.1, 152.7 151.2, 133.8, 131.9, 128.5, 124.6, 124.2, 120.8, 113.8, 111.7, 111.3, 77.9, ca. 40.64-39.36 (overlapped with solvent), 30.23. ^{15}N NMR (DMSO-d_6 from $MeNO_2$) δ:

-211.89, -245.63, -319.77. ^{19}F NMR (DMSO-d_6 from $CFCl_3$) δ: -134.64. $C_{18}H_{18}BF_2N_3O$, Calcd. C 63.37, H 5.32, N 12.32; Found C 63.30, H 5.44, N 12.30.

1,1-difluoro-3-phenyl-1*H*-benzo[4,5]oxazolo[3,2-*c*][1,3,2]oxazaborinin-10-ium-1-uide (**X=O, R=H**) - Yellowish-green solid, yield 38%, Mp 239.2–240.8°C. ^{1}H NMR (DMSO-d_6 from TMS) δ: 8.12 (m, 2H), 7.94 (m, 1H), 7.72 (m, 1H) 7.65 (m, 1H), 7.59 (m, 4H), 7.55 (d, 1H, $^3J_{H,H}$=1.64 Hz), 7.22 (s, 1H). ^{11}B NMR (DMSO-d_6 from $BF_3{\cdot}Et_2O$) δ: 1.85, (t). ^{13}C NMR δ: 170.8, 165.1, 148.5, 133.1, 130.1, 129.5, 127.5, 126.9, 126.4, 114.9, 112.5, 82.1. ^{15}N NMR (DMSO-d_6 from $MeNO_2$) δ: -213.54. ^{19}F NMR (DMSO-d_6 from $CFCl_3$) δ: -135.07. $C_{15}H_{10}BF_2NO_2$, Calcd. C 63.20, H 3.54, N 4.91; Found C 63.25, H 3.49, N 4.83.

3-(4-(dimethylamino)phenyl)-1,1-difluoro-1*H*-benzo[4,5]oxazolo[3,2-*c*][1,3,2]oxazaborinin-10-ium-1-uide (**X=O, R=NMe$_2$**) - Orange solid, yield 41%, Mp 298–300°C. ^{1}H NMR (DMSO-d_6 from TMS) δ: 7.96 (d, 2H, $^3J_{H,H}$=9.12 Hz), 7.85 (d, 1H, $^3J_{H,H}$=7.36 Hz), 7.61 (d, 1H, $^3J_{H,H}$=7.64 Hz), 7.50 (m, 2H), 6.89 (s, 1H), 6.81 (d, 2H, $^3J_{H,H}$=9.16 Hz), 3.07 (s, 6H). ^{11}B NMR (DMSO-d_6 from $BF_3{\cdot}Et_2O$) δ: 1.79, (t). ^{13}C NMR δ: 172.1 153.7, 152.4, 148.2, 130.6, 129.6, 127.0, 125.9, 119.1, 114.2, 112.1, 111.8, 77.7, ca. 40.61-39.35 (overlapped with solvent). ^{15}N NMR (DMSO-d_6 from $MeNO_2$) δ: -313.97. ^{19}F NMR (DMSO-d_6 from $CFCl_3$) δ: -133.19. $C_{17}H_{15}BF_2N_2O_2$, Calcd. C 62.23, H 4.61, N 8.54; Found C 62.14, H 4.64, N 8.39.

1,1-difluoro-3-phenyl-1*H*-benzo[4,5]thiazolo[3,2-*c*][1,3,2]oxazaborinin-10-ium-1-uide (**X=S, R=H**) - Yellow solid, yield 43% Mp 244.5–245.7°C. ^{1}H NMR (DMSO-d_6 from TMS) δ: 8.23 (d, 1H, $^3J_{H,H}$=8.0 Hz), 8.13 (m, 2H), 8.00 (d, 1H, $^3J_{H,H}$=8.16 Hz) 7.69 (m, 1H), 7.59 (m, 4H), 7.51 (s, 1H). ^{11}B NMR (DMSO-d_6 from $BF_3{\cdot}Et_2O$) δ: 1.64 (t). ^{13}C NMR δ: 169.3, 164.9, 142.1, 133.1, 132.8, 129.5, 129.4, 128.9, 127.3, 126.6, 124.1, 117.8, 90.8. ^{15}N NMR (DMSO-d_6 from $MeNO_2$) δ: -186.16. ^{19}F NMR (DMSO-d_6 from $CFCl_3$) δ: -132.16. $C_{15}H_{10}BF_2NOS$, Calcd. C 59.83, H 3.35, N 4.65. Found C 59.75, H 3.43, N 4.54.

3-(4-(dimethylamino)phenyl)-1,1-difluoro-1*H*-benzo[4,5]thiazolo[3,2-*c*][1,3,2]oxazabor-

inin-10-ium-1-uide (**X=S, R=NMe$_2$**) - Yellow solid, yield 44%, Mp 280–283°C. ^{1}H NMR (DMSO-d$_6$ from TMS) δ: 8.17 (d, 1H, $^3J_{H,H}$=8.0 Hz), 7.89 (m, 2H), 7.85 (s, 1H) 7.61 (m, 1H), 7.47 (m, 1H), 7.23 (s, 1H), 6.82 (d, 2H), 3.06 (s, 1H). ^{11}B NMR (DMSO-d$_6$ from $BF_3{\cdot}Et_2O$) δ: 1.54 (t). ^{13}C NMR δ: 168.5, 166.5, 153.5, 142.3, 129.4, 128.5, 125.7, 123.8, 118.8, 117.1, 111.9, 87.6, ca. 40.60-39.35 (overlapped with solvent). ^{15}N NMR (DMSO-d$_6$ from $MeNO_2$) δ: -194.22, -314.90. ^{19}F NMR (DMSO-d$_6$ from $CFCl_3$) δ: -133.09. $C_{17}H_{15}BF_2N_2OS$, Calcd. C 59.32, H 4.39, N 8.14. Found C 59.43, H 4.45, N 8.06.

Acknowledgments

B.O. and A.M.G. thank the Polish National Science Centre (Grant No. 2017/26/M/ST5/00327). W.B. acknowledges the statutory activity subsidy from the Polish Ministry of Science and Higher Education for the Faculty of Chemistry of Wrocław University of Technology. The authors want to address special and warm gratitude to Dr Robert Zaleśny from Faculty of Chemistry, Wrocław University of Science and Technology for countless valuable discussions which helped to improve manuscript and his kind and precious help with CC2 calculations. Authors are also very graceful to Damian Plazuk from University of Łódź for recording fluorescence quantum yield with the use of the integrating sphere. The calculations were performed at the Wroclaw Center for Networking and Supercomputing.

Supporting Informations

The Supporting Information is available on the Elsevier website. It contains fluorescence decay curves, NMR spectra, Cartesian coordinates, computational results and bond-lenghts analysis.

References

[1] I. Kaya, M. Yildirim, A. Avci, Synthesis and characterization of fluorescent polyphenol species derived from methyl substituted aminopyridine based schiff bases: The effect of substituent position

on optical, electrical, electrochemical, and fluorescence properties, Synth. Met. 160 (9-10) (2010) 911–920.

[2] A. Zakrzewska, R. Zaleśny, E. Kolehmainen, B. Ośmiałowski, B. Jędrzejewska, H. Ågren, M. Pietrzak, Substituent effects on the photophysical properties of fluorescent 2-benzoylmethylenequinoline difluoroboranes: A combined experimental and quantum chemical study, Dyes Pigm. 99 (2013) 957–965.

[3] K.-Y. Chen, H.-Y. Tsai, W.-C. Lin, H.-H. Chu, Y.-C. Weng, C.-C. Chan, Esipt fluorescent dyes with adjustable optical properties: Substituent and conjugation effects, J. Lumin. 154 (2014) 168–177.

[4] T. Yoshida, T. Furuyama, M. Asai, N. Kobayashi, Fluorescence enhancement of tetraazaporphyrins by the use of bulky substituent effects, Chem. Lett. 44 (8) (2015) 1056–1058.

[5] M.-S. Tsai, C.-L. Ou, C.-J. Tsai, Y.-C. Huang, Y.-C. Cheng, S.-S. Sun, J.-S. Yang, Fluorescence enhancement of unconstrained gfp chromophore analogues based on the push-pull substituent effect, J. Org. Chem. 82 (15) (2017) 8031–8039.

[6] D. Wang, X. Fan, S. Sun, S. Du, H. Li, J. Zhu, Y. Tang, M. Chang, Y. Xu, Substituent effect: A new strategy to construct a ratiometric fluorescent probe for detection of al^{3+} and imaging in vivo, Sens. Actuator B-Chem. 264 (2018) 304–311.

[7] T. Uppal, X. Hu, F. Fronczek, S. Maschek, P. Bobadova-Parvanova, M. Vicente, Synthesis, computational modeling, and properties of benzo-appended bodipys, Chem. Eur. J. 18 (13) (2012) 3893–3905.

[8] Y. Ni, W. Zeng, K.-W. Huang, J. Wu, Benzene-fused bodipys: synthesis and the impact of fusion mode, Chem. Commun. 49 (12) (2013) 1217–1219.

[9] S.-I. Kato, T. Furuya, M. Nitani, N. Hasebe, Y. Ie, Y. Aso, T. Yoshihara, S. Tobita, Y. Nakamura, A series of π-extended thiadiazoles fused with electron-donating heteroaromatic moieties: Synthesis, properties, and polymorphic crystals, Chem. Eur. J. 21 (7) (2015) 3115–3128.

[10] J. Golden, J. Facendola, D. Sylvinson, C. Baez, P. Djurovich, M. Thompson, Boron dipyridylmethene (dipyr) dyes: Shedding light on pyridine-based chromophores, J. Org. Chem. 82 (14) (2017) 7215–7222.

[11] O. Kim, J. Jang, H. Kim, S. Han, G. Tsui, J. Joo, Synthesis of fluorescent indazoles by palladium-catalyzed benzannulation of pyrazoles with alkynes, Org. Lett. 19 (6) (2017) 1450–1453.

[12] W.-Q. Zhang, K. Cheng, X. Yang, Q.-Y. Li, H. Zhang, Z. Ma, H. Lu, H. Wu, X.-J. Wang, A benzothiadiazole-based fluorescent sensor for selective detection of oxalyl chloride and phosgene, Org. Chem. Front. 4 (9) (2017) 1719–1725.

[13] G. Li, K.-J. Jiang, Y.-F. Li, S.-L. Li, L.-M. Yang, Efficient structural modification of triphenylamine-based organic dyes for dye-sensitized solar cells, J. Phys. Chem. C 112 (30) (2008)

11591–11599.

[14] G. De Miguel, M. Wielopolski, D. Schuster, M. Fazio, O. Lee, C. Haley, A. Ortiz, L. Echegoyen, T. Clark, D. Guldi, Triazole bridges as versatile linkers in electron donor-acceptor conjugates, J. Am. Chem. Soc. 133 (33) (2011) 13036–13054.

[15] A. Fihey, A. Perrier, W. R. Browne, D. Jacquemin, Multiphotochromic molecular systems, Chem. Soc. Rev. 44 (2015) 3719–3759.

[16] A. Grabarz, A. D. Laurent, B. Jędrzejewska, A. Zakrzewska, D. Jacquemin, B. Ośmiałowski, The influence of the π-conjugated spacer on photophysical properties of difluoroboranyls derived from amides carrying a donor group, J. Org. Chem. 81 (2016) 2280–2292.

[17] M. M. Alcaide, F. M. F. Santos, V. F. Pais, J. I. Carvalho, D. Collado, E. Pérez-Inestrosa, J. F. Arteaga, F. Boscá, P. M. P. Gois, U. Pischel, Electronic and functional scope of boronic acid derived salicylidenehydrazone (bashy) complexes as fluorescent dyes, J. Org. Chem. 82 (14) (2017) 7151–7158.

[18] C. Flors, I. Oesterling, T. Schnitzler, E. Fron, G. Schweitzer, M. Sliwa, A. Herrmann, M. van der Auweraer, F. C. de Schryver, K. Müllen, J. Hofkens, Energy and electron transfer in ethynylene bridged perylene diimide multichromophores, J. Phys. Chem. C 111 (12) (2007) 4861–4870.

[19] X. Lv, T. Li, Q. Wu, C. Yu, L. Jiao, E. Hao, Polybrominated bophy dyes: Synthesis, reactivity, and properties, J. Org. Chem. 83 (3) (2018) 1134–1145.

[20] P. Wei, J.-X. Zhang, Z. Zhao, Y. Chen, X. He, M. Chen, J. Gong, H.-Y. Sung, I. Williams, J. Lam, B. Tang, Multiple yet controllable photoswitching in a single aiegen system, J. Am. Chem. Soc. 140 (5) (2018) 1966–1975.

[21] X. Chen, T. Pradhan, F. Wang, J. Kim, J. Yoon, Fluorescent chemosensors based on spiroring-opening of xanthenes and related derivatives, Chem. Rev. 112 (3) (2012) 1910–1956.

[22] I. Astakhova, J. Wengel, Interfacing click chemistry with automated oligonucleotide synthesis for the preparation of fluorescent dna probes containing internal xanthene and cyanine dyes, Chem. Eur. J. 19 (3) (2013) 1112–1122.

[23] A. Pandey, A. Kumar, S. Vishwakarma, K. Upadhyay, A highly specific 'turn-on' fluorescent detection of mg^{2+} through a xanthene based fluorescent molecular probe, RSC Adv. 6 (8) (2016) 6724–6729.

[24] S. Ma, Y. Wang, M. She, S. Wang, Z. Yang, P. Liu, S. Zhang, J. Li, Design strategies and progress on xanthene-based fluorescent probe for metal ions, Reviews in Anal. Chem. 36 (2).

[25] K. More, T.-H. Lim, S.-Y. Kim, J. Kang, K.-S. Inn, D.-J. Chang, Characteristics of new bioreductive fluorescent probes based on the xanthene fluorophore: Detection of nitroreductase and imaging of hypoxic cells, Dyes Pigm. 151 (2018) 245–253.

[26] L. Yuan, W. Lin, K. Zheng, L. He, W. Huang, Far-red to near infrared analyte-responsive fluo-

rescent probes based on organic fluorophore platforms for fluorescence imaging, Chem. Soc. Rev. 42 (2) (2013) 622–661.

[27] G. Cheng, J. Fan, W. Sun, J. Cao, C. Hu, X. Peng, A near-infrared fluorescent probe for selective detection of hclo based on se-sensitized aggregation of heptamethine cyanine dye, Chem. Commun. 50 (8) (2014) 1018–1020.

[28] J. Yin, Y. Kwon, D. Kim, D. Lee, G. Kim, Y. Hu, J.-H. Ryu, J. Yoon, Cyanine-based fluorescent probe for highly selective detection of glutathione in cell cultures and live mouse tissues, J. Am. Chem. Soc. 136 (14) (2014) 5351–5358.

[29] A. Nano, A. Boynton, J. Barton, A rhodium-cyanine fluorescent probe: Detection and signaling of mismatches in dna, J. Am. Chem. Soc. 139 (48) (2017) 17301–17304.

[30] X. Wang, J. Lv, X. Yao, Y. Li, F. Huang, M. Li, J. Yang, X. Ruan, B. Tang, Screening and investigation of a cyanine fluorescent probe for simultaneous sensing of glutathione and cysteine under single excitation, Chem. Commun. 50 (97) (2014) 15439–15442.

[31] G. Ulrich, R. Ziessel, A. Harriman, The chemistry of fluorescent bodipy dyes: versatility unsurpassed, Angew. Chem. Int. Ed. 47 (7) (2008) 1184–1201.

[32] N. Boens, V. Leen, W. Dehaen, Fluorescent indicators based on bodipy, Chem. Soc. Rev. 41 (3) (2012) 1130–1172.

[33] Y. Ni, J. Wu, Far-red and near infrared bodipy dyes: synthesis and applications for fluorescent ph probes and bio-imaging, Org. Biomol. Chem. 12 (23) (2014) 3774–3791.

[34] F. Wang, L. Zhou, C. Zhao, R. Wang, Q. Fei, S. Luo, Z. Guo, H. Tian, W.-H. Zhu, A dual-response bodipy-based fluorescent probe for the discrimination of glutathione from cystein and homocystein, Chem. Sci. 6 (4) (2015) 2584–2589.

[35] Q. Fei, M. Li, J. Chen, B. Shi, G. Xu, C. Zhao, X. Gu, Design of bodipy-based near-infrared fluorescent probes for h_2s, J. Photochem. Photobiol. A 355 (2018) 305–310.

[36] H. Jung, P. Kwon, J. Lee, J. Kim, C. Hong, J. Kim, S. Yan, J. Lee, J. Lee, T. Joo, J. Kim, Coumarin-derived cu^{2+}-selective fluorescence sensor: Synthesis, mechanisms, and applications in living cells, J. Am. Chem. Soc. 131 (5) (2009) 2008–2012.

[37] H. Jung, K. Ko, G.-H. Kim, A.-R. Lee, Y.-C. Na, C. Kang, J. Lee, J. Kim, Coumarin-based thiol chemosensor: Synthesis, turn-on mechanism, and its biological application, Org. Lett. 13 (6) (2011) 1498–1501.

[38] J. Li, C.-F. Zhang, S.-H. Yang, W.-C. Yang, G.-F. Yang, A coumarin-based fluorescent probe for selective and sensitive detection of thiophenols and its application, Anal. Chem. 86 (6) (2014) 3037–3042.

[39] V. Gupta, N. Mergu, L. Kumawat, A. Singh, Selective naked-eye detection of magnesium (ii) ions using a coumarin-derived fluorescent probe, Sens. Actuator B-Chem. 207 (2015) 216–223.

[40] L. Wang, W. Li, W. Zhi, D. Ye, Y. Wang, L. Ni, X. Bao, A rapid-responsive fluorescent probe based on coumarin for selective sensing of sulfite in aqueous solution and its bioimaging by turn-on fluorescence signal, Dyes Pigm. 147 (2017) 357–363.

[41] R. Ziessel, G. Ulrich, A. Harriman, The chemistry of bodipy: A new *El Dorado* for fluorescence tools, New J. Chem. 31 (2007) 496–501.

[42] M. A. Potopnyk, R. Lytvyn, Y. Danyliv, M. Ceborska, O. Bezvikonnyi, D. Volyniuk, J. V. Gražulevičius, N,o π-conjugated 4-substituted 1,3-thiazole bf_2 complexes: Synthesis and photophysical properties, J. Org. Chem. 83 (3) (2018) 1095–1105.

[43] D. Frath, K. Benelhadj, M. Munch, J. Massue, G. Ulrich, Polyanils and polyboranils: Synthesis, optical properties, and aggregation-induced emission, J. Org. Chem. 81 (20) (2016) 9658–9668.

[44] L. Weber, D. Eickhoff, A. Chrostowska, C. Darrigan, H.-G. Stammler, B. Neumann, Synthesis, structure, and properties of luminescent diazaborole and indole systems, Chem. Heterocycl. Compd. 53 (1) (2017) 54–65.

[45] K. Zhang, H. Zheng, C. Hua, M. Xin, J. Gao, Y. Li, Novel fluorescent n,o-chelated fluorineboron benzamide complexes containing thiadiazoles: Synthesis and fluorescence characteristics, Tetrahedron 74 (2018) 4161–4167.

[46] C. Yu, E. Hao, T. Li, J. Wang, W. Sheng, Y. Wei, X. Mu, L. Jiao, Dipyrrolylquinoxaline difluoroborates with intense red solid-state fluorescence, Dalton Trans. 44 (2015) 13897–13905.

[47] G. Ulrich, S. Goeb, A. De Nicola, P. Retailleau, R. Ziessel, Chemistry at boron: Synthesis and properties of red to near-ir fluorescent dyes based on boron-substituted diisoindolomethene frameworks, J. Org. Chem. 76 (11) (2011) 4489–4505.

[48] Y. Ni, W. Zeng, K.-W. Huang, J. Wu, Benzene-fused bodipys: synthesis and the impact of fusion mode, Chem. Commun. 49 (2013) 1217–1219.

[49] A. Skotnicka, P. Czeleń, R. Gawinecki, Tautomeric equilibria in solutions of 1-methyl-2-phenacylbenzimidazoles, J. Mol. Struct. 1134 (2017) 546–551.

[50] A. M. Grabarz, B. Jędrzejewska, A. Zakrzewska, R. Zaleśny, A. D. Laurent, D. Jacquemin, B. Ośmiałowski, Photophysical properties of phenacylphenantridine difluoroboranyls: effect of substituent and double benzannulation, J. Org. Chem. 82 (3) (2017) 1529–1537.

[51] W. Sheng, J. Cui, Z. Ruan, L. Yan, Q. Wu, C. Yu, Y. Wei, E. Hao, L. Jiao, [a]-phenanthrene-fused bf_2 azadipyrromethene (azabodipy) dyes as bright near-infrared fluorophores, J. Org. Chem. 82 (2017) 10341–10349.

[52] A. B. Descalzo, H.-J. Xu, Z. Shen, K. Rurack, Influence of the meso-substituent on strongly red emitting phenanthrene-fused boron-dipyrromethene (bodipy) fluorophores with a propeller-like conformation, J. Photochem. Photobiol. A 352 (2018) 98–105.

[53] X.-D. Jiang, X. Liu, T. Fang, C. Sun, L. Xiao, Synthesis and photophysical properties of long wave-

length absorbing bodipy/aza-bodipy bearing a five-membered ring, Tetrahedron Lett. 59 (2018) 546–549.

[54] W. Zhao, E. Carreira, Conformationally restricted aza-bodipy: Highly fluorescent, stable near-infrared absorbing dyes, Chem. Eur. J. 12 (27) (2006) 7254–7263.

[55] R. Gresser, M. Hummert, H. Hartmann, K. Leo, M. Riede, Synthesis and characterization of near-infrared absorbing benzannulated aza-bodipy dyes, Chem. Eur. J. 17 (10) (2011) 2939–2947.

[56] J. Min, T. Ameri, R. Gresser, M. Lorenz-Rothe, D. Baran, A. Troeger, V. Sgobba, K. Leo, M. Riede, D. Guldi, C. Brabec, Two similar near-infrared (ir) absorbing benzannulated aza-bodipy dyes as near-ir sensitizers for ternary solar cells, ACS Appl. Mater. Interfaces 5 (12) (2013) 5609–5616.

[57] A. Diaz-Moscoso, E. Emond, D. Hughes, G. Tizzard, S. Coles, A. Cammidge, Synthesis of a class of core-modified aza-bodipy derivatives, J. Org. Chem. 79 (18) (2014) 8932–8936.

[58] J. Karlsson, A. Harriman, Origin of the red-shifted optical spectra recorded for aza-bodipy dyes, J. Phys. Chem. A 120 (16) (2016) 2537–2546.

[59] D. Frath, S. Azizi, G. Ulrich, P. Retailleau, R. Ziessel, Facile synthesis of highly fluorescent boranil complexes, Org. Lett. 13 (13) (2011) 3414–3417.

[60] D. Frath, S. Azizi, G. Ulrich, R. Ziessel, Chemistry on boranils: An entry to functionalized fluorescent dyes, Org. Lett. 14 (18) (2012) 4774–4777.

[61] G. N. Lipunova, E. V. Nosova, V. N. Charushin, O. N. Chupakhin, Boron(iii) complexes with n,n'- and n,o-heterocyclic ligands: Synthesis and spectroscopic properties, Comments Inorg. Chem. 36 (5) (2016) 245–303.

[62] M. Urban, K. Durka, P. Jankowski, J. Serwatowski, S. Luliński, Highly fluorescent red-light emitting bis(boranils) based on naphthalene backbone, J. Org. Chem. 82 (15) (2017) 8234–8241.

[63] J. Massue, D. Frath, G. Ulrich, P. Retailleau, R. Ziessel, Synthesis of luminescent 2-(2'-hydroxyphenyl)benzoxazole (hbo) borate complexes, Org. Lett. 14 (1) (2012) 230–233.

[64] J. Massue, G. Ulrich, R. Ziessel, Effect of 3,5-disubstitution on the optical properties of luminescent 2-(2' -hydroxyphenyl)benzoxazoles and their borate complexes, Eur. J. Org. Chem. (25) (2013) 5701–5709.

[65] K. Benelhadj, J. Massue, P. Retailleau, S. Chibani, B. Le Guennic, D. Jacquemin, R. Ziessel, G. Ulrich, Solution- and solid-state luminescent borate complexes based on a substituted π-conjugated 2-(6'-hydroxy-5'-benzofuryl) scaffold, Eur. J. Org. Chem. (32) (2014) 7156–7164.

[66] S. Xu, R. E. Evans, T. Liu, G. Zhang, J. N. Demas, C. O. Trindle, C. L. Fraser, Aromatic difluoroboron β-diketonate complexes: Effects of π-conjugation and media on optical properties, Inorg. Chem. 52 (7) (2013) 3597–3610.

[67] A. D'Aleo, F. Fages, Boron difluoride complexes of 3-hydroxyflavone derivatives: efficient bioin-

771 spired dyes for solution and solid-state emission, Photochem. Photobiol. Sci. 12 (2013) 500–510.
772 [68] B. Štefane, F. Požgan, E. Kim, E. Choi, J.-C. Ribierre, J. W. Wu, M. Ponce-Vargas, B. L. Guennic,
773 D. Jacquemin, G. Canard, E. Zaborova, F. Fages, A. D'Aléo, Ethynylene-analogues of hemicur-
774 cuminoids: Synthesis and ground- and excited properties of their boron difluoride complexes, Dyes
775 Pigm. 141 (2017) 38–47.
776 [69] M. Santra, H. Moon, M.-H. Park, T.-W. Lee, Y. K. Kim, K. H. Ahn, Dramatic substituent effects
777 on the photoluminescence of boron complexes of 2-(benzothiazol-2-yl)phenols, Chem. Eur. J. 18
778 (2012) 9886–9893.
779 [70] U. Balijapalli, A. Joseph, S. Chinduluri, E. Shanmugam, K. Sathiyanarayanan, Luminescent
780 tetrahydrodibenzo[a,i]phenanthridin-5-yl)phenol-boron complexes (borophenanthridines), Dyes
781 Pigm. 137 (2017) 182–190.
782 [71] Y. Kubota, M. Tsukamoto, K. Ohnishi, J. Jin, K. Funabiki, M. Matsui, Synthesis and fluorescence
783 properties of novel squarylium-boron complexes, Org. Chem. Front. 4 (2017) 1522–1527.
784 [72] J. Dobkowski, P. Wnuk, J. Buczyńska, M. Pszona, G. Orzanowska, D. Frath, G. Ulrich, J. Massue,
785 S. Mosquera-Vázquez, E. Vauthey, C. Radzewicz, R. Ziessel, J. Waluk, Substituent and solvent
786 effects on the excited state deactivation channels in anils and boranils, Chem. Eur. J. 21 (2014)
787 1312–1327.
788 [73] Y. Wu, W. Yuan, H. Ji, Y. Qin, J. Zhang, H. Li, Y. Li, Y. Wang, Y. Sun, W. Liu, New fluorescent
789 imidazo[1,2-α]pyridine-bodipy chromophores: Experimental and theoretical approaches, and cell
790 imaging exploration, Dyes Pigm. 142 (2017) 330–339.
791 [74] W. Chen, L. Zhu, Y. Hao, X. Yue, J. Gai, Q. Xiao, S. Huang, J. Sheng, X. Song, Detection of
792 thiophenol in buffer, in serum, on filter paper strip, and in living cells using a red-emitting amino
793 phenothiazine boranil based fluorescent probe with a large stokes shift, Tetrahedron 73 (31) (2017)
794 4529–4537.
795 [75] A. Loudet, K. Burgess, Bodipy dyes and their derivatives: Syntheses and spectroscopic properties,
796 Chem. Rev. 107 (11) (2007) 4891–4932.
797 [76] U. Balijapalli, K. Sathiyanarayanan, Synthesis and optical properties of a series of green-light-
798 emitting 2-(4-phenylquinolin-2-yl)phenol-bf_2 complexes (boroquinols), Eur. J. Org. Chem. (23)
799 (2015) 5089–5098.
800 [77] S. Deshpande, H. Kumbhar, G. Shankarling, Photoswitchable conjugated assembly involving flu-
801 orescent boranil, J. Lumin. 179 (2016) 314–321.
802 [78] B. Jędrzejewska, A. Zakrzewska, G. Młostoń, Š. Budzák, K. Mroczyńska, A. M. Grabarz, M. A.
803 Kaczorowska, D. Jacquemin, B. Ośmiałowski, Synthesis and photophysical properties of novel
804 donor-acceptor n-(pyridin-2-yl)-substituted benzo(thio)amides and their difluoroboranyl deriva-
805 tives, J. Phys. Chem. A (24) (2016) 4116–4123.

[79] Z. Xu, G. Ding, G. Zhong, G. Xing, F. Li, W. Huang, H. Tian, Color tunable organic light-emitting diodes using coumarin dopants, Res. Chem. Intermed. 34 (2) (2008) 249–256.

[80] V. S. Padalkar, A. Tathe, V. D. Gupta, V. S. Patil, K. Phatangare, N. Sekar, Synthesis and photo-physical characteristics of esipt inspired 2-substituted benzimidazole, benzoxazole and benzothiazole fluorescent derivatives, J. Fluoresc. 22 (1) (2012) 311–322.

[81] A. Skotnicka, E. Kolehmainen, P. Czeleń, A. Valkonen, R. Gawinecki, Synthesis and structural characterization of substituted 2-phenacylbenzoxazoles, Int. J. Mol. Sci. 14 (3) (2013) 4444–4460.

[82] B. Ośmiałowski, A. Zakrzewska, B. Jędrzejewska, A. Grabarz, R. Zaleśny, W. Bartkowiak, E. Kolehmainen, Influence of substituent and benzoannulation on photophysical properties of 1-benzoylmethyleneisoquinoline difluoroborates, J. Org. Chem. 80 (2015) 2072–2080.

[83] A. M. Brouwer, Standards for photoluminescence quantum yield measurements in solution (iupac technical report), Pure Appl. Chem. 83 (2011) 2213–2011.

[84] J. Tomasi, M. Persico, Molecular interactions in solution: An overview of methods based on continuous distributions of the solvent, Chem. Rev. 94 (7) (1994) 2027–2094.

[85] T. Schwabe, K. Sneskov, J. Haugaard Olsen, J. Kongsted, O. Christiansen, C. Hättig, Peri-cc2: A polarizable embedded ri-cc2 method, J. Chem. Theory Comput. 8 (9) (2012) 3274–3283.

[86] C. M. Breneman, K. B. Wiberg, Determining atom-centered monopoles from molecular electrostatic potentials. the need for high sampling density in formamide conformational analysis, J. Comput. Chem. 11 (1990) 361–373.

[87] J. Wang, R. M. Wolf, J. W. Caldwell, P. A. Kollman, D. A. Case, Development and testing of a general amber force field, J. Comput. Chem. 25 (2004) 1157–1174.

[88] D. C. et al., AMBER 16, university of California, San Francisco (2016).

[89] TURBOMOLE V7.0 2015, a development of University of Karlsruhe and Forschungszentrum Karlsruhe GmbH, 1989-2007, TURBOMOLE GmbH, since 2007; available from `http://www.turbomole.com` (last accessed 01 apr. 17).

[90] M. J. Frisch, G. W. Trucks, H. B. Schlegel, G. E. Scuseria, M. A. Robb, J. R. Cheeseman, G. Scalmani, V. Barone, B. Mennucci, G. A. Petersson, H. Nakatsuji, M. Caricato, X. Li, H. P. Hratchian, A. F. Izmaylov, J. Bloino, G. Zheng, J. L. Sonnenberg, M. Hada, M. Ehara, K. Toyota, R. Fukuda, J. Hasegawa, M. Ishida, T. Nakajima, Y. Honda, O. Kitao, H. Nakai, T. Vreven, J. A. Montgomery, Jr., J. E. Peralta, F. Ogliaro, M. Bearpark, J. J. Heyd, E. Brothers, K. N. Kudin, V. N. Staroverov, R. Kobayashi, J. Normand, K. Raghavachari, A. Rendell, J. C. Burant, S. S. Iyengar, J. Tomasi, M. Cossi, N. Rega, J. M. Millam, M. Klene, J. E. Knox, J. B. Cross, V. Bakken, C. Adamo, J. Jaramillo, R. Gomperts, R. E. Stratmann, O. Yazyev, A. J. Austin, R. Cammi, C. Pomelli, J. W. Ochterski, R. L. Martin, K. Morokuma, V. G. Zakrzewski, G. A. Voth, P. Salvador, J. J. Dannenberg, S. Dapprich, A. D. Daniels, Ö. Farkas, J. B. Foresman, J. V.

Ortiz, J. Cioslowski, D. J. Fox, Gaussian 2009, gaussian Inc. Wallingford CT 2009.

[91] A. D. Becke, Density-functional exchange-energy approximation with correct asymptotic behavior, Phys. Rev. A 38 (1988) 3098–3100. doi:10.1103/PhysRevA.38.3098.

[92] C. Lee, W. Yang, R. G. Parr, Development of the colle-salvetti correlation-energy formula into a functional of the electron density, Phys. Rev. B 37 (1988) 785–789. doi:10.1103/PhysRevB.37.785.
URL http://link.aps.org/doi/10.1103/PhysRevB.37.785

[93] A. D. Becke, Density-functional thermochemistry. iii. the role of exact exchange, J. Chem. Phys. 98 (7) (1993) 5648–5652. arXiv:http://dx.doi.org/10.1063/1.464913, doi:10.1063/1.464913.
URL http://dx.doi.org/10.1063/1.464913

[94] C. Adamo, V. Barone, Toward reliable density functional methods without adjustable parameters: The pbe0 model, J. Chem. Phys. 110 (13) (1999) 6158–6170. arXiv:http://dx.doi.org/10.1063/1.478522, doi:10.1063/1.478522.
URL http://dx.doi.org/10.1063/1.478522

[95] M. Ernzerhof, G. E. Scuseria, Assessment of the perdew-burke-ernzerhof exchange-correlation functional, J. Chem. Phys. 110 (11) (1999) 5029–5036. arXiv:http://dx.doi.org/10.1063/1.478401, doi:10.1063/1.478401.
URL http://dx.doi.org/10.1063/1.478401

[96] Y. Zhao, D. G. Truhlar, The m06 suite of density functionals for main group thermochemistry, thermochemical kinetics, noncovalent interactions, excited states, and transition elements: two new functionals and systematic testing of four m06-class functionals and 12 other functionals, Theor. Chem. Acc. 120 (1) (2008) 215–241. doi:10.1007/s00214-007-0310-x.
URL http://dx.doi.org/10.1007/s00214-007-0310-x

[97] A. D. Becke, A new mixing of hartree-fock and local density-functional theories, J. Chem. Phys. 98 (2) (1993) 1372–1377. arXiv:http://dx.doi.org/10.1063/1.464304, doi:10.1063/1.464304.
URL http://dx.doi.org/10.1063/1.464304

[98] T. Yanai, D. P. Tew, N. C. Handy, A new hybrid exchange-correlation functional using the coulomb-attenuating method (cam-b3lyp), Chem. Phys. Lett. 393 (1–3) (2004) 51–57. doi:http://dx.doi.org/10.1016/j.cplett.2004.06.011.
URL http://www.sciencedirect.com/science/article/pii/S0009261404008620

[99] J.-D. Chai, M. Head-Gordon, Systematic optimization of long-range corrected hybrid density functionals, J. Chem. Phys. 128 (8) (2008) 084106. arXiv:http://dx.doi.org/10.1063/1.2834918, doi:10.1063/1.2834918.
URL http://dx.doi.org/10.1063/1.2834918

[100] J.-D. Chai, M. Head-Gordon, Long-range corrected hybrid density functionals with damped atom–atom dispersion corrections, Phys. Chem. Chem. Phys. 10 (2008) 6615–6620.

doi:10.1039/B810189B.
URL http://dx.doi.org/10.1039/B810189B

[101] H. Iikura, T. Tsuneda, T. Yanai, K. Hirao, A long-range correction scheme for generalized-gradient-approximation exchange functionals, J. Chem. Phys. 115 (8) (2001) 3540–3544. arXiv:http://dx.doi.org/10.1063/1.1383587, doi:10.1063/1.1383587.
URL http://dx.doi.org/10.1063/1.1383587

[102] Y. Zhao, D. G. Truhlar, Density functional for spectroscopy: No long-range self-interaction error, good performance for rydberg and charge-transfer states, and better performance on average than b3lyp for ground states, J. Phys. Chem. A 110 (49) (2006) 13126–13130. arXiv:http://dx.doi.org/10.1021/jp066479k, doi:10.1021/jp066479k.
URL http://dx.doi.org/10.1021/jp066479k

[103] Y. Zhao, D. G. Truhlar, Comparative dft study of van der waals complexes: Rare-gas dimers, alkaline-earth dimers, zinc dimer, and zinc-rare-gas dimers, J. Phys. Chem. A 110 (15) (2006) 5121–5129. arXiv:http://dx.doi.org/10.1021/jp060231d, doi:10.1021/jp060231d.
URL http://dx.doi.org/10.1021/jp060231d

[104] T. Le Bahers, C. Adamo, I. Ciofini, A qualitative index of spatial extent in charge-transfer excitations, J. Chem. Theory Comput. 7 (8) (2011) 2498–2506.

[105] D. Jacquemin, T. Le Bahers, C. Adamo, I. Ciofini, What is the "best" atomic charge model to describe through-space charge-transfer excitations?, Phys. Chem. Chem. Phys. 14 (2012) 5383–5388.

[106] T. H. Dunning, Gaussian basis sets for use in correlated molecular calculations. i. the atoms boron through neon and hydrogen, J. Chem. Phys. 90 (1989) 1007–1023.

[107] R. A. Kendall, T. H. Dunning, R. J. Harrison, Electron affinities of the first-row atoms revisited. systematic basis sets and wave functions, J. Chem. Phys. 96 (1992) 6796–6806.

[108] D. E. Woon, T. H. Dunning, Gaussian basis sets for use in correlated molecular calculations. iv. calculation of static electrical response properties, J. Chem. Phys. 100 (1994) 2975–2988.

[109] J. R. Lakowicz, Principles of Fluorescence Spectroscopy, 3rd edition, Springer, 2006.

[110] G. V. Bünau, J. b. birks: Photophysics of aromatic molecules. wiley-interscience, london 1970. 704 seiten. preis: 210s, Berichte der Bunsengesellschaft für physikalische Chemie 74 (12) (1970) 1294–1295.

[111] A. G. Al-Sehemi, M. Pannipara, A. Kalam, A. M. Asiri, A combined experimental and computational investigation on spectroscopic and photophysical properties of a coumarinyl chalcone, J. Fluoresc. 26 (4) (2016) 1357–1365.

[112] G. Garcia, C. Adamo, I. Ciofini, Evaluating push-pull dye efficiency using td-dft and charge transfer indices, Phys. Chem. Chem. Phys. 15 (2013) 20210–20219.

[113] S. S. Bag, M. K. Pradhan, R. Kundu, S. Jana, Highly solvatochromic fluorescent naphthalimides: Design, synthesis, photophysical properties and fluorescence switch-on sensing of ct-dna, Bioorganic Med. Chem. Lett. 23 (1) (2013) 96–101.

[114] O. A. Kucherak, L. Richert, Y. Mély, A. S. Klymchenko, Dipolar 3-methoxychromones as bright and highly solvatochromic fluorescent dyes, Phys. Chem. Chem. Phys. 14 (2012) 2292–2300.

[115] W. A. Wassam, E. C. Lim, "proximity effect" in radiationless transitions, J. Chem. Phys. 68 (2) (1978) 433–454.

[116] S. Fery-Forgues, M. T. Le Bris, J. C. Mialocq, J. Pouget, W. Rettig, B. Valeur, Photophysical properties of styryl derivatives of aminobenzoxazinones, J. Phys. Chem. 96 (2) (1992) 701–710.

[117] V. Gulbinas, G. Kodis, S. Jursenas, L. Valkunas, A. Gruodis, J.-C. Mialocq, S. Pommeret, T. Gustavsson, Charge transfer induced excited state twisting of n,n-dimethylaminobenzylidene-1,3-indandione in solution, J. Phys. Chem. A 103 (20) (1999) 3969–3980.

[118] K. Rurack, M. L. Dekhtyar, J. L. Bricks, U. Resch-Genger, W. Rettig, Quantum yield switching of fluorescence by selectively bridging single and double bonds in chalcones: Involvement of two different types of conical intersections, J. Phys. Chem. A 103 (48) (1999) 9626–9635.

[119] A. M. Asiri, S. A. El-Daly, S. A. Khan, Spectral characteristics of 4-(p-n,n-dimethylaminophenylmethylene)-2-phenyl-5-oxazolone (dpo) in different media, Spectrochim. Acta A 95 (2012) 679 – 684.

[120] B. Jędrzejewska, P. Krawczyk, M. Józefowicz, Experimental and theoretical studies of the influence of solvent polarity on the spectral properties of two push-pull oxazol-5-(4h)-one compounds, Spectrochim. Acta A 171 (2017) 258 – 267.

[121] D. Jacquemin, V. Wathelet, E. Perpéte, C. Adamo, Extensive td–dft benchmark: Singlet-excited states of organic molecules, J. Chem. Theory Comput. 5 (2009) 2420–2435.

[122] A. Laurent, D. Jacquemin, Td–dft benchmarks: A review, Int. J. Quant. Chem. 113 (2013) 2019–2039.

[123] D. Jacquemin, Excited-state dipole and quadrupole moments: Td–dft versus cc2, J. Chem. Theory Comput. 12 (8) (2016) 3993–4003.

[124] C. Guido, B. Mennucci, G. Scalmani, D. Jacquemin, Excited state dipole moments in solution: Comparison between state-specific and linear-response td–dft values, J. Chem. Theory. Comput. 14 (3) (2018) 1544–1553.

[125] D. Nardi, A. Tajana, R. Pennini, Heterocyclic compounds from 3,3-dimercapto-1-aryl-2-propen-1-ones. note 2. condensation with o-aminothophenol and o-aminophenol, J. Heterocycl. Chem. 12 (1) (1975) 139–142.

[126] H. Stachel, Die darstellung einiger heterocyclen aus acylketen-derivaten (benzoxazole, benzothiazole, benzothiodiazine, chinazolone). über keten–derivate, x, Arch. Pharm. 296 (5) (1963) 337–343.

[127] (Du Pont de Nemours and Co., 1939, U.S. Patent 2323504, Preparation of omega-acyl-azoles).

[128] F. Stepanov, S. Davydowa, Heterocyclic derivatives of methylketones, Zh. Obshch. Khim. 28 (1958) 891–896.

[129] F. Babichev, Y. Volovenko, Acylalation of 2-methylbenzazoles with use of esters of carboxylic acids, Sov. Prog. Chem. 43 (1977) 49–50.

[130] E. Rauch, P. Dickinson, J. Welsh, Prepartion of 2-benzoylmethylbezoxazoles (1968, U.S. Patent 3375258).

[131] E. H. Sund, B. E. Donohue, T. K. Thomas, Synthesis of 2-(2-benzoxazolyl)-1-phenylethanone and related ethanones, J. Chem. Eng. Data 24 (3) (1979) 253–253.

[132] R. A. M. O'Ferrall, B. A. Murray, ^{1}h and ^{13}c nmr spectra of α-heterocyclic ketones and assignment of keto, enol and enaminone tautomeric structures, J. Chem. Soc. Perkin Trans. 2 (1994) 2461–2470.

[133] I. Dzvinchuk, M. Lozinskii, A. Vypirailenko, C-mono- and dibenzoylation of 2-methylbenzimidazole with use of benzoyl chloride, Zh. Org. Khim. 30 (1994) 909–914.

[134] G. Ciurdaru, M. Ciuciu, The acylation of 2-methylbenzazoles, J. Prakt. Chem. 321 (2) (1979) 320–322.

[135] H. De Silva, S. Chatterjee, W. Henry, C. Pittman, Synthesis of functionalized fused-ring heterocycles from tautomers of 2-(thiazole, oxazole, benzothaizole, and benzoxazole)-1-phenylethenols and 1,3-diacyl chlorides or n-(chlorocarbonyl) isocyanate, Synthesis 44 (2012) 3453–3464.

[136] H. De Silva, W. Henry, C. Pittman, Reactions of keto-enol tautomers of 2-thiazolyl-, 2-oxazolyl-, 2-benzoxazolyl-, or 2-benzothiazolyl-1-phenylethenols with α,β-alkynyl esters: Syntheses of highly functionalized fused-ring heterocycles, Synthesis 44 (2012) 3337–3352.

[137] E. R. T. Robinson, D. M. Walden, C. Fallan, M. D. Greenhalgh, P. H.-Y. Cheong, A. D. Smith, Non-bonding 1,5-s$\cdots$o interactions govern chemo- and enantioselectivity in isothiourea-catalyzed annulations of benzazoles, Chem. Sci. 7 (2016) 6919–6927.

[138] Z.-T. Huang, M.-X. Wang, A new route to 3h-1,5-benzodiazepines and heterocylic ketene aminals from benzoyl substituted ketene dithioacetals and diamines, Synthesis 12 (1992) 1273–1276.

[139] Z.-T. Huang, M.-X. Wang, The synthesis and tautomerization of ketene aminals with benzimidazoline ring, Tetrahedron 48 (1992) 2325–2332.

[140] J. Davoll, 58. the reaction of o-phenylenediamine with $\alpha\beta$-unsaturated acids and with β-keto-esters, J. Chem. Soc. (1960) 308–314.

[141] I. Dzvinchuk, A. M. Nesterenko, V. V. Polovinko, A. B. Ryabitskii, M. Lozinskii, Synthesis and tautomerism of 2-phenacyl-1h-benzimidazoles and their hydrogen bromide salts, Chem. Heterocycl. Compd. 47 (2011) 953–963.

[142] Y. Kubota, S. Tanaka, K. Funabiki, M. Matsui, Synthesis and fluorescence properties of thiazole-

boron complexes bearing a β-ketoiminate ligand, Org. Lett. 14 (2012) 4682–4685.

[143] Q. Liu, X. Wang, H. Yan, Y. Wu, Z. Li, S. Gong, P. Liu, Z. Liu, Benzothiazole-enamide-based bf_2 complexes: luminophores exhibiting aggregation-induced emission, tunable emission and highly efficient solid-state emission, J. Mater. Chem. C 3 (2015) 2953–2959.

[144] L. F. Minuti, M. G. Memeo, S. Crespi, P. Quadrelli, Fluorescent probes from stable aromatic nitrile oxides, Eur. J. Org. Chem. (4) (2015) 821–829.

[145] A. Matviitsuk, J. E. Taylor, D. B. Cordes, A. M. Z. Slawin, A. D. Smith, Enantioselective stereodivergent nucleophile-dependent isothiourea-catalysed domino reactions, Chem. Eur. J. 22 (2016) 17748–17757.

[146] M. V. Costa, A. Brembilla, D. Roizard, P. Lochon, Action of (2-benzothiazolyl) methyllithium with organic polar functions, J. Heterocycl. Chem. 28 (1991) 1541–1544.

[147] Z. Zhang, T. Daynard, S. Wang, X. Du, G. Chopiuk, J. Yan, J. Chen, S. Sviridov, Pyrazolylbenzothiazole derivatives and their use as therapeutic agents (2004, Patent WO2004/11460).